Memoirs of the Faculty of Science, Kyoto University, Series of Physics, Astrophysics, Geophysics and Chemistry, Vol.XXXXIII, No.1, Article 3,2002

Stark Structure and Field Ionization Characteristics of Highly Excited Rydberg Atoms

By

Yasuhiro Kishimoto

Nuclear Science Division, Institute for Chemical Research, Kyoto University
Gokasho, Uji, Kyoto 611-0011, Japan

(*December 17, 2001)*

Abstract

The Stark structure and time evolution of highly excited ^{85}Rb Rydberg states in a pulsed electric field have been studied experimentally as well as theoretically. The Rydberg states in ^{85}Rb with the principal quantum number n ranging from 110 to 140 have been excited with the two step laser excitation scheme and field ionization spectra under the pulsed electric field were observed with the ionized electron detection. From the systematic measurements it was found that the in general there exist two peaks in the field ionization spectrum: the lower peak is rather broad and the field value of the peak does not depend on the excitation position in the manifold. The value of the higher peak field, on the other hand, increases with increasing bluer states in the manifold when the pulsed electric field is increased in the same direction with the initially applied static field. However when the pulsed field is increased in the reversed direction to the static field, the peak field value decreases with increasing bluer state excitations, showing the opposite behavior to the case in the same field-driving direction.

In order to reveal the origin of these two peak-field values in the ionization process, theoretical calculations of the Stark structure and ionization rates in an electric field have been performed with a computational method based on the Hamiltonian diagonalization. From these calculations it was found that the excitation position dependence of the higher peaks observed in the field ionization is in good agreement with the predictions from the tunneling process. On the other hand

the lower peak behavior is roughly explained from the autoionization-like process together with the effect of the blackbody-induced radiative transitions to the neighboring states from the originally excited states.

In due course of the above investigations, time evolution of the multi-level Rydberg system in a pulsed electric field was also studied to confirm the usefulness and applicabilities of the present method of theoretical calculations. Specifically the transition probabilities in the first avoided crossing at which the $113p_{3/2}$ state crosses the bluest state in the 110 manifold was measured and compared with the theoretical predictions obtained from a newly developed formalism on the time evolution of multi-level Rydberg system. The experimental results are in good agreement with the predictions. The opposite behavior in the excitation-position dependence of the higher ionization peak-field between the same and the reversed driving directions of the pulsed electric field was also found to be well explained with the present theoretical treatment in the time evolution, thus showing that the present theoretical treatment is quite satisfactory even in such highly excited Rydberg atoms.

Contents

1 Introduction

Highly excited Rydberg states [1] have many interesting properties and provide ideal and versatile situations in various fields of physics. In particular, the Rydberg atoms couple strongly to the electromagnetic field, thus they have played important roles in cavity quantum electrodynamics (cavity QED) [2] and its related applications in the fields of fundamental physics. Specifically the realization of the single atom maser is one of the most important contributions of the Rydberg atoms to these fields. The quantum computing and related quantum measurement experiments being actively developed recently are also some of the mostly attractive and exciting fields in the application of the Rydberg atoms.

The Rydberg atoms have been also suggested to be useful and actually used for a quite sensitive single-photon detector [3, 4, 5]. Figger *et al.* demonstrated that the Rydberg atoms can be used as a sensitive detector of 100 GHz microwave blackbody radiations [4]. We have developed and are carrying out a large-scale dark matter axion search experiment CARRACK, where the highly excited Rydberg atoms are used to detect microwave photons produced by the conversion of axions into photons in a strong magnetic field via the Primakoff process [6, 7, 8, 9, 10].

In these experiments covering a wide range of fundamental physics fields, Rydberg states have been mostly detected by the selective field ionization method, in which atoms are subjected to an externally applied electric field in a static or a pulsed form; due to the strong coupling to the electric field, the atoms are easily ionized in a weak electric field, especially for the highly excited states.

Extensive experimental and theoretical investigations have been performed for the detailed understanding of the structure of Rydberg states and the characteristics of field ionizations: specifically the Stark energy level structure in a static field, including polarizabilities and dynamical properties in a pulsed electric field are some of the mostly interested subjects so far.

The energy level structure of Rydberg states in an electric field was first studied in detail by Zimmerman *et al.* [11]. They calculated the Stark energy structure of alkali atoms with the principal quantum number $n = 15$ by diagonalizing the Hamiltonian matrix. They also carried out experiments in which the laser excitation spectra and field ionization characteristics were investigated. The theoretical results of the energy level structure agree well with the experimental ones and thus the agreement shows validity and usefulness of their calculation method. Also from their experimental study they remarked for the first time that an autoionization-like process of the field ionization is important especially for the blue states in the non-hydrogenic

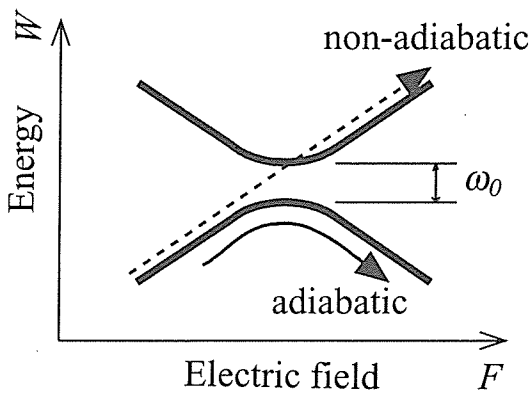

Figure 1: Two Stark levels with an avoided crossing of ω_0. If the field is driven through the avoided crossing in a long time compared to $1/\omega_0$, the passage is adiabatic(solid arrow), while if it is driven rapidly, the passage is non-adiabatic(broken arrow).

atoms in addition to the usual tunneling process [12].

Harmin, on the other hand, developed an analytical method to calculate the Stark structure and photoabsorption cross sections and applied the method to some alkali atoms around $n \sim 15$ [13, 14].

Time evolution of the Rydberg states in a pulsed electric field is also one of the attractive subjects, since they provide an interesting and ideal, yet accessible case for the quantum system evolution with many potential-energy curves that cross one another [15]. From the experimental side, on the other hand, it is essential for understanding the detailed behavior of the field ionization processes and thus for providing the efficient way to detect the Rydberg states selectively.

When considering the time evolution in a time varying electric field, it is inevitably important to take into account the avoided crossings between many Stark states: Increasing the electric field, the energy levels shift and cross (avoided crossing) each other as illustrated in Fig. 1 for the two level crossing. On the crossing point, they traverse adiabatically or non-adiabatically, depending on the slew rate. If the traversal is completely adiabatic, the initial state passes along the solid line. If the crossing is completely non-adiabatic, it passes along the broken line. Since in the real situation both transitions occur with certain probabilities depending on the slew rate in each crossing, the populated levels are generally distributed between these two extreme paths in the actual case with many Stark levels.

In a two-level system the avoided crossing can be approximately treated with the Landau-Zener-Stückelberg (LZS) process theoretically. Many groups have obtained good agreement between the observed crossing behavior and the LZS formula. Rubbmark *et al.*, for example, studied the dynamics of traversing avoided crossings between $n = 18$ and $n = 19$ manifolds in Li as a function of the slew rate [16]. They extended the LZS method to be applicable to the case of an arbitrary waveform of the applied electric pulse for the two level crossing, and they compared and discussed the resulting theoretical behavior with the experimental data.

Harmin examined the coherent time evolution of a Rydberg Stark system on a grid of LZS avoided-crossings under a linear ramped electric field in which infinite number of manifold levels are treated as linear in time, parallel and equally spaced. The time evolution of an initially populated state is then governed by the two-level LZS transitions at avoided crossings and adiabatic evolution between them [15]. In such a system it was suggested that the coherent process arising from the constructive enhancement in the population of some particular levels plays an important role in the development of the field ionization process.

In the last stage of increasing the electric field, the atoms are finally ionized. Two ionization processes have been known to occur in general: 1) the tunneling process and 2) the autoionization-like process, which is due to the interaction of a bound blue state in the core region with continuum red states belonging to some upper n manifold. The process 2) occurs only in non-hydrogenic atoms. As n increases, the process 2) is expected to be less important compared to the process 1) because the interactions in the core becomes weaker with increasing n.

The above results on the Stark properties of Rydberg states were mostly obtained from the study of Rydberg states with n lower than ~ 50, and no detailed studies on the still higher excited Rydberg states with $n > 80$ have been reported so far. This situation is partly due to the increasing difficulty in the selective detection of a particular Rydberg state among many close-lying states on the experimental side. On the theoretical side, on the other hand, larger number of Stark states have to be taken into account at higher n, and thus theoretical treatment is increasingly complicated and time consuming.

In order to circumvent the above situation, systematic investigations on the Stark properties of the highly excited Rydberg states of ^{85}Rb with n ranging up to ~ 140 were initiated both experimentally and theoretically: specifically we applied various forms of an electric field pulse to the electrodes, and studied the resulting field ionization behavior and the time evolution characteristics of the Rydberg states. Also we developed theoretical methods to calculate the Stark structure and to trace the time evolution in the multi-

level Stark system.

Along this line of investigations, we have developed an experimental method with which a low angular-momentum state is selectively ionized and detected from other angular momentum states by applying a pulsed electric field [17]. Our method opens an efficient way to selectively ionize highly excited states, and thus enables us to apply the highly excited Rydberg states to fundamental research area.

In this paper, detailed experimental studies of the time evolution of the highly excited Rydberg states and of the following field ionization process are reported with theoretical analyses. Specifically we measured the threshold electric field value for the ionization of the highly excited Rydberg states of ^{85}Rb with n ranging from 110 to 140 in a pulsed field regime. Adiabatic and non-adiabatic transition probabilities at the first avoided crossing of a np state with the adjacent manifold were also measured as a function of the slew rate of the applied electric field. From these experimental studies, it was found that, in general, there exist two peaks in the ionization field: the lower peak is rather broad and the field value of the peak does not depend on the excitation position in the manifold. The value of the higher peak field, on the other hand, increases with increasing bluer states (that is, blue states approaching nearer to the bluest states) in the manifold when the pulsed electric field is increased in the same direction with the initially applied static field. However when the pulsed field is increased in the reversed direction to the static field, the peak field decreases with increasing bluer state excitations, showing the opposite behavior to the case in the same field-driving direction.

In order to reveal the origin of these two peak fields in the ionization processes, theoretical calculations of the Stark structure and ionization rates in an electric field have been performed with a computational method based on the Hamiltonian diagonalization. Here the calculations of the radial matrix elements were done with the quantum defect theory under the Coulomb approximation. From these calculations it was found that the excitation position dependence of the higher peak observed in the field ionization is in good agreement with the predictions from the tunneling process. On the other hand the lower peak behavior is roughly explained from the autoionization-like process together with the effect of the blackbody-induced radiative transitions to the neighboring states from the originally excited states.

In due course of the above investigations, time evolution of the multi-level Rydberg system in a pulsed electric field was also studied to confirm the usefulness and applicabilities of the present method of theoretical calculations. Specifically the transition probabilities in the first avoided crossings of ^{85}Rb between the $113p$ state and the bluest states in the 110 manifold were mea-

sured and compared with the theoretical predictions obtained from a newly developed formalism on the time evolution of the multi-level Rydberg system. The experimental results are in good agreement with the predictions.

Also the multi-level formalism of the time evolution was applied to the case of the zero-field crossing: except the low angular momentum states with $\ell \leq 3$, the levels with the same n are all degenerated approximately at zero field in alkali atoms. When the applied pulsed-field is reversed from the initial direction during the ionization process, the manifold levels are once driven to zero field and then again to the higher field region. The predicted ionization behavior in such a situation is also in good agreement with experimental results.

Following the brief review of the Rydberg atoms, theoretical formulations on the Stark structure calculations and on the trace of the time evolution are presented in Sec. 3. Experimental procedure and the results are shown in Secs. 4 and 5 together with the comparison with the theoretical predictions. Section 6 is devoted to the discussions on the results and then the conclusions of the present investigation are described in Sec. 7.

2 Rydberg Atoms

Rydberg atoms are the highly excited atoms near to the ionization limit with a large principal quantum number n. The binding energy is given by the Rydberg formula,

$$W_{n\ell} = R/(n - \delta_\ell)^2 = R/n^{*2}, \tag{1}$$

where R is the Rydberg constant, 13.6 eV, δ_ℓ is the quantum defect of the states with angular momentum ℓ and $n^* = n - \delta_\ell$ is the effective principal quantum number. For low ℓ states, the penetration and polarization of the ionic core by the valence electron lead to large quantum defects and to strong departures from the hydrogenic behavior. As ℓ increases, an orbit of the valence electron becomes more circular and the atom becomes more hydrogenic.

The Rydberg atoms have following characteristics: 1)small energy differences between n and $n+1$ levels, 2)large $E1$ transition rates between n and $n+1$ levels and 3)long lifetimes.

The energy difference between the adjacent Rydberg states is given by $\Delta W_n = W_{n+1} - W_n \approx R/n^{*3}$ and lies in the microwave range. In the case of $n \sim 100$, for example, the transition frequency is around 7 GHz.

The Rydberg atom strongly couples to the electromagnetic field in the microwave range. The transition rate in vacuum between n and $n+1$ states

is given by

$$\Gamma_n \left(\sec^{-1}\right) \approx 10^5 n^{*4} \left(\Delta W_n \left(\mathrm{eV}\right)\right)^3. \tag{2}$$

In the case of $n \sim 100$, the rate is estimated to be 3×10^4 $\sec^{-1}$.

The radiative lifetime induced by the blackbody radiation is given by

$$\tau_n^{BB} = 2.03 \times 10^{-7} (n^*)^2 \frac{300\,\mathrm{K}}{T}. \tag{3}$$

The lifetime at room temperature for the state with $n \sim 100$ is estimated to be 2 msec.

Now we consider the Rydberg states of a hydrogenic atom at first. The most straightforward way to treat the Stark effect in the hydrogenic atom is to use parabolic coordinates, in which the problem remains separable even with an electric field. In the electric field F, the potential term is given by

$$V(r) = -\frac{1}{r} + Fz. \tag{4}$$

In parabolic coordinates the Shrödinger equation for an electron in the potential of Eq. (4) is written as,

$$\Psi(\xi, \eta) = \frac{1}{\sqrt{\xi\eta}} \Xi(\xi) H(\eta), \tag{5}$$

$$\frac{d^2\Xi(\xi)}{d\xi^2} - \left(\frac{m^2-1}{4\xi^2} - \frac{Z_1}{\xi} - \frac{W}{2} + \frac{F}{4}\xi\right)\Xi(\xi) = 0, \tag{6}$$

$$\frac{d^2H(\eta)}{d\eta^2} - \left(\frac{m^2-1}{4\eta^2} - \frac{Z_2}{\eta} - \frac{W}{2} - \frac{F}{4}\eta\right) H(\eta) = 0, \tag{7}$$

where Z_1 and Z_2 are the separation constants and both are related by $Z_1 + Z_2 = 1$. With the first order perturbation, the energy of the Rydberg state in the electric field is expressed as,

$$W_{nn_1n_2m} = -\frac{1}{2n^2} + \frac{3}{2} F n (n_1 - n_2), \tag{8}$$

where n_1 and n_2 are the parabolic quantum numbers and related to the principal quantum number n and the magnetic quantum number m by

$$n = n_1 + n_2 + |m| + 1. \tag{9}$$

Equation (8) shows that the states with n in zero field split into $(n - 1 - |m|)$ levels in an electric field. The set of $(n - 1 - |m|)$ degenerated states is called "manifold". The states with higher energy in manifold, *i.e.* the states

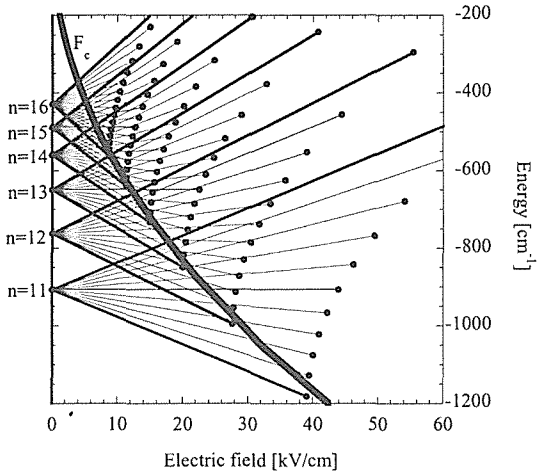

Figure 2: Stark energy shift and the ionization threshold in a hydrogenic atom with n=11-16, m=0. The thin lines show the energy levels in an electric field. Closed circles show the ionization fields by the tunneling process F_{Z_2}. The bold line shows the classical ionization limit F_c.

with $n_1 - n_2 \sim n$, are called "blue" states, and those with $n_1 - n_2 \sim -n$ are called "red" states.

The quantum number n_1 and n_2 are related to the separation parameters,

$$Z_1 = \frac{1}{n}\left(n_1 + \frac{|m|+1}{2}\right), \tag{10}$$

$$Z_2 = \frac{1}{n}\left(n_2 + \frac{|m|+1}{2}\right). \tag{11}$$

We use the difference of the separation parameters $Z_1 - Z_2$ to express the energy level in manifold. For the bluest, the central and the reddest states with $n_1 - n_2 \sim +n$, 0 and $-n$, the value of $Z_1 - Z_2$ has $\sim +1$, 0 and -1, respectively. The Stark structure of a hydrogenic atom is shown in Fig. 2.

As the field strength increases, the bluest state with n and the reddest state with $(n+1)$ cross. The crossing occurs at the field strength,

$$F = \frac{1}{3n^5} = 0.17\left(\frac{100}{n}\right) \text{V/cm}. \tag{12}$$

The binding energy of a valence electron decreases as n^{-2} and thus the Rydberg states are strongly affected by the external electric field owing to the

large dipole moment. The potential $V(r)$ has a saddle point at $z = 1/\sqrt{F}$, at which the potential value is

$$V_{\max} = -2\sqrt{F}. \tag{13}$$

If the electron is bound by an energy W, a field given by

$$F = \frac{W^2}{4} \tag{14}$$

is adequate for the ionization to occur classically. This field value is usually termed the classical field for ionization. When ignoring the energy shift in the electric field, W is given by $-1/2n^2$, then we obtain the familiar result,

$$F_c = \frac{1}{16n^4} = 3.2 \times \left(\frac{100}{n}\right)^4 \text{V/cm}. \tag{15}$$

This classical picture is useful to roughly estimate the field value to ionize a state. The bold solid line in Fig. 2 shows the classical ionization threshold F_c.

The classical picture, however, has serious defects. First, Eq. (15) ignores the Stark shift, and second, the classical approach ignores the spatial distribution of the wavefunction. In parabolic coordinates, the motion in the ξ direction is bound in any value of the field. Thus for ionization to occur the electron must escape to infinity in the η direction. Classically, the ionization only occurs for the energy above the peak of the potential,

$$V(\eta) = \frac{m^2 - 1}{4\eta^2} - \frac{Z_2}{\eta} - \frac{W}{2} - \frac{F}{4}\eta. \tag{16}$$

Ignoring the short range η^{-2} term, a good approximation for low $|m|$, we find that the required field for ionization is

$$F_{Z_2} = \frac{W^2}{4Z_2}. \tag{17}$$

The separation parameter Z_2 is around $1/n$ for a blue state, $Z_2 \sim 1/2$ for a central state, and $Z_2 \sim 1$ for a red state, thus, among these states in manifold, the reddest one will most easily be ionized. For the extreme red state, we find the threshold field strength,

$$F_{Z_2 \sim 1} = \frac{1}{9n^4}, \tag{18}$$

and for the extreme blue one, the ionization field strength is given by

$$F_{Z_2 \sim n} = \frac{1}{21n^4}. \tag{19}$$

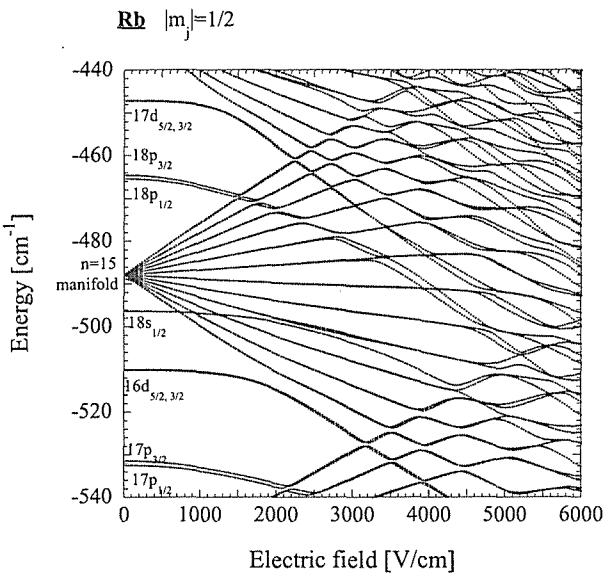

Figure 3: Stark structure of ^{85}Rb with n=15, $|m_j| = 1/2$ calculated with the present theoretical treatment.

The ionization threshold F_{Z_2} calculated with Eq. (17) are shown by closed circles in Fig. 2.

Atoms other than H have characteristics essentially similar to those of H atom in an electric field, but there are important differences due to the presence of the finite-sized ionic core.

Figure 3 shows the energy diagram of ^{85}Rb with $n = 15$ and $|m_j| = 1/2$ in an electric field. It is noted that the degeneracy of low ℓ states, the s, p and d states, is resolved in zero field, and the p state locates above the manifold and the s and d states below the manifold in ^{85}Rb. The second effect of the presence of the finite-sized ionic core (*i.e.* the presence of the nonzero quantum defects) is that n_1 is not a good quantum number and blue and red states are coupled with each other by the overlap at the core. When the field strength reaches $1/3n^5$, blue and red states with adjacent n do not cross as they do in H, but exhibit an avoided crossing.

The avoided crossings affect the time evolution of the system in a pulsed ionization field. If the crossing is traversed fast compared to the inverse of the separation energy between the states, $1/\omega_0$, the traversal is non-adiabatic. The probability of the non-adiabatic transition in an isolated two level system

is given by the Landau-Zener-Stückelberg formula,

$$P = \exp(-2\pi \frac{S_x}{S}). \tag{20}$$

Here S_x is defined by

$$S_x = \frac{\omega_0^2}{\left(\frac{dW_1}{dF} - \frac{dW_2}{dF}\right)}, \tag{21}$$

where dW_1/dF and dW_2/dF are the Stark shifts for each level and S is the time differential of the electric field, $S = dF/dt$. The adiabatic and non-adiabatic transitions are discussed later in detail in Sec. 3.3.2.

Another effect of the finite-sized ionic core is the coupling between a blue state which would be stable in H and red states which are unbound. This coupling modifies the ionization lifetime in an electric field. Due to this coupling, a blue state has a finite probability to be ionized at a field less than the value expected from the tunneling process. The ionization rate of this process is later discussed more in detail in Sec. 3.4.2.

3 Theory

3.1 Overview

In order to understand more quantitatively the Stark structure and dynamical behavior of highly excited Rydberg states under a pulsed electric field, a numerical method to be applicable to such highly excited states was developed based on the direct diagonalization of Hamiltonians. Firstly the Stark energy level structure was calculated with a basis set including the fine structure interactions. This treatment is necessary especially in the present investigations because the fine structure effect cannot be neglected in heavier atoms like Rb which is the atom we have studied here.

With the obtained energy eigenvalues and the eigenstates in the applied electric field, radiative lifetimes and ionization rates in the electric field can be calculated. We have calculated the ionization rates and hence the lifetimes of the Rydberg states in an electric field in the two processes, that is, in the tunneling and the autoionization-like processes. In the calculations on the tunneling process, we adopted a semi-empirical calculation developed by Damburg and Kolosov [18] from its simplicity, yet with enough accuracy for the present purpose. More accurate calculations based on "the density of states" method by Luc-Koenig and Bachelier [19] are also discussed in some detail.

On the other hand, detailed calculations on the ionization rate due to the autoionization-like process were performed by taking into account also the effect of the fine structure interactions with the wavefunctions obtained from the Hamiltonian diagonalization.

Time evolution of a multi-level Rydberg system in a time varying electric field was also calculated based on a newly obtained formalism. This computational method was applied to the first avoided crossing of the $113p_{3/2}$ state with the bluest states in the 110 manifold. Energy eigenvalues and their eigenstates in electric fields provide the interaction strength and the energy gap at the avoided crossings, thus this kind of analysis gives quantitative test for the applicabilities of the present theoretical calculations.

3.2 Calculation of energy levels in an electric field based on Hamiltonian diagonalization

The Hamiltonian of an alkali atom in an electric field F is given by,

$$\begin{aligned} H &= \frac{1}{2m}p^2 - \frac{1}{r} + V_d + \Lambda + Fz \\ &= H_0 + Fz, \end{aligned} \tag{22}$$

where V_d is the difference between the potential of the alkali atom and the Coulomb potential and Λ is the fine structure interaction. The term Λ is especially important for heavy alkali atoms. These terms, V_d and Λ, are only nonzero near $r = 0$. For the non-hydrogenic atom, the parabolic representation does not provide an attractive basis for the Stark problem as is the case of a hydrogenic atom. This is because, due to the presence of V_d and Λ, the Hamiltonian matrix in zero field is not diagonal in the parabolic basis. On the other hand, it is diagonal in the $|n\ell jm_j\rangle$ basis. For this reason we have chosen to work with the $|n\ell jm_j\rangle$ basis.

It is important to realize that the perturbative treatment of the Stark energy with the power-series expansion in a field is fundamentally inadequate because the expansion does not converge. A straightforward and effective method of calculating the energy in an electric field is the direct diagonalization of the Hamiltonian matrix. Specifically the matrix elements of H_0, including V_d and Λ, are diagonalized in the $|n\ell jm_j\rangle$ basis with quantum defect theory. The diagonal matrix elements are given by the Rydberg formula,

$$\langle n\ell jm_j|H_0|n\ell jm_j\rangle = \frac{R_{\rm alk}}{(n-\delta_{n\ell j})^2} \tag{23}$$

$$= \frac{R_{\rm alk}}{(n^*)^2}, \tag{24}$$

Table 1: ^{85}Rb quantum defect parameters [20].

Series	δ_0	δ_2	δ_4	δ_6	δ_8
$ns_{1/2}$	3.13109(2)	0.204(8)	-1.8		
$np_{1/2}$	2.65456(15)	0.388(60)	-7.904	116.437	-405.907
$np_{3/2}$	2.64145(20)	0.33(18)	-0.97495	14.6001	-44.7265
$np_{3/2,5/2}$	1.347157(80)	-0.59553(18)	-1.50517	-2.4206	19.736

where $R_{\rm alk}$ is the Rydberg constant for the alkali atom, $\delta_{n\ell j}$ is the quantum defect of an $n\ell j$ state and n^* is the effective quantum number. The value of $\delta_{n\ell j}$ is given by

$$\delta_{n\ell j} = \delta_0 + \frac{\delta_2}{(n-\delta_0)^2} + \frac{\delta_4}{(n-\delta_0)^4} + \frac{\delta_6}{(n-\delta_0)^6} + \frac{\delta_8}{(n-\delta_0)^8}\cdots, \tag{25}$$

where δ_0, $\delta_2\ldots$ are experimentally determined parameters for the alkali atoms. The parameters δ_0, $\delta_2\ldots$ in Eq. (25) for ^{85}Rb are tabulated in Table 1 [20]. The virtue of the quantum defect theory is that we need not know the details of the radial dependence of V_d and Λ, which are not known exactly.

Off-diagonal matrix elements are expressed by the $|n\ell jm_j\rangle$ basis:

$$\begin{aligned}
&\langle n^*\ell jm_j|Fz|n^{*\prime}\ell' j'm_j'\rangle \\
= \;& F\delta(m_j,m_j')\delta(\ell,\ell'\pm 1)\langle n^*\ell|r|n^{*\prime}\ell\pm 1\rangle \\
&\cdot \sum_{m_\ell=m_j\pm m_s} \langle \ell,\frac{1}{2},m_\ell,m_s|j,m_j\rangle\langle \ell',\frac{1}{2},m_\ell,m_s|j,m_j\rangle \\
&\cdot\langle \ell,m_\ell|\hat{z}|\ell\pm 1,m_\ell\rangle,
\end{aligned} \tag{26}$$

where the first two factors in the sum are Clebsch-Gordan coefficients and $\hat{z} = z/|z|$. The angular part of the matrix elements are derived by using algebra of spherical harmonics,

$$\begin{aligned}
\langle \ell,m_\ell|\hat{z}|\ell-1,m_\ell\rangle &= \sqrt{\frac{\ell^2-m_\ell^2}{(2\ell+1)(2\ell-1)}}, \\
\langle \ell,m_\ell|\hat{z}|\ell+1,m_\ell\rangle &= \sqrt{\frac{(\ell+1)^2-m_\ell^2}{(2\ell+3)(2\ell+1)}}.
\end{aligned} \tag{27}$$

The computational task is to evaluate the radial dipole matrix elements. They are calculated under the Coulomb approximation following the method

by Davydikin and Zon [21],

$$\begin{aligned}
&\langle n^*\ell|r|n'^*\ell \pm 1\rangle \\
&= \frac{\bar{n}^*}{\Delta Z}\left\{\frac{\sin\pi\Delta}{\pi\Delta}\left[\Delta(1-\varepsilon) \mp \frac{\sqrt{1-\varepsilon^2}}{\varepsilon}\right]\right\} \\
&\quad + \frac{\bar{n}^*}{\Delta Z}\left\{\frac{d}{dx}J_\Delta(-x) \pm \frac{\sqrt{1-\varepsilon^2}}{\varepsilon}J_\Delta(-x)\right\}, \qquad (28)
\end{aligned}$$

$$\bar{n}^* = \sqrt{n^* n^{*\prime}}, \qquad (29)$$

$$\bar{\ell} = \frac{\ell + \ell'}{2}, \qquad (30)$$

$$\varepsilon = \sqrt{1 - \frac{(\bar{\ell} + 1/2)^2}{(\bar{n}^*)^2}}, \qquad (31)$$

$$\Delta = n^{*\prime} - n^*, \qquad (32)$$

$$x = \varepsilon\Delta, \qquad (33)$$

$$J_\Delta(S) = \frac{1}{\pi}\int_0^\pi \cos(\Delta\theta - S\sin\theta)d\theta. \qquad (34)$$

Equation (28) is an analytic expression for the dipole matrix elements corresponding to transitions between Rydberg states with $|\Delta| \ll n^*, n^{*\prime}$. We note here that the approximation used in Eq. (28) is more accurate when n^* becomes larger and thus it gives quite good results for the Rydberg states with $n > 100$. Accuracy of the calculation of the radial elements is discussed later in Sec. 6.3.

The last task is diagonalizing the Hamiltonian matrix to obtain the eigenvalues and eigenstates in each electric field. Figures 4 - 6 show the calculated energy level structure of the Rydberg states of ^{85}Rb around $n = 110$ manifold of $|m_j| = 1/2$, $3/2$ and $5/2$ in the electric field. In this calculation, the terms included in the basis set of the diagonalization are $105 \leq n \leq 115$ for each $|m_j|$. This basis set is adequate within the calculated range of the field, up to 0.3 V/cm. This point is discussed further in Sec. 6.3.

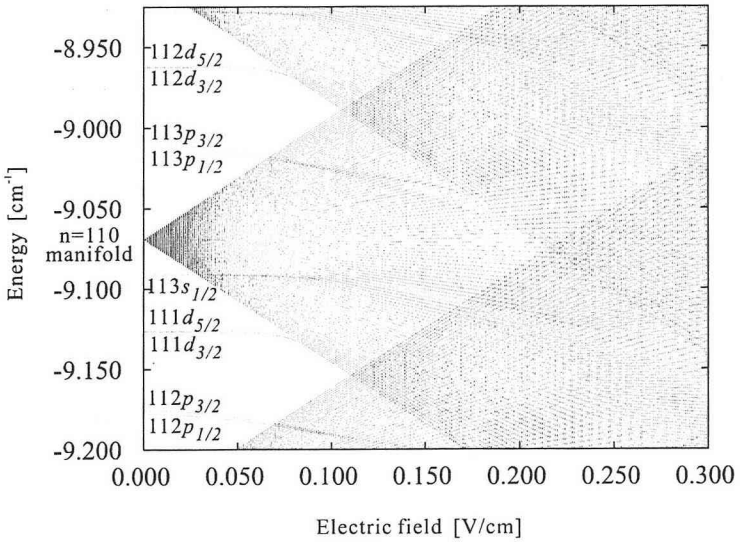

Figure 4: Calculated Stark energy structure of ^{85}Rb for $n = 110, |m_j| = 1/2$.

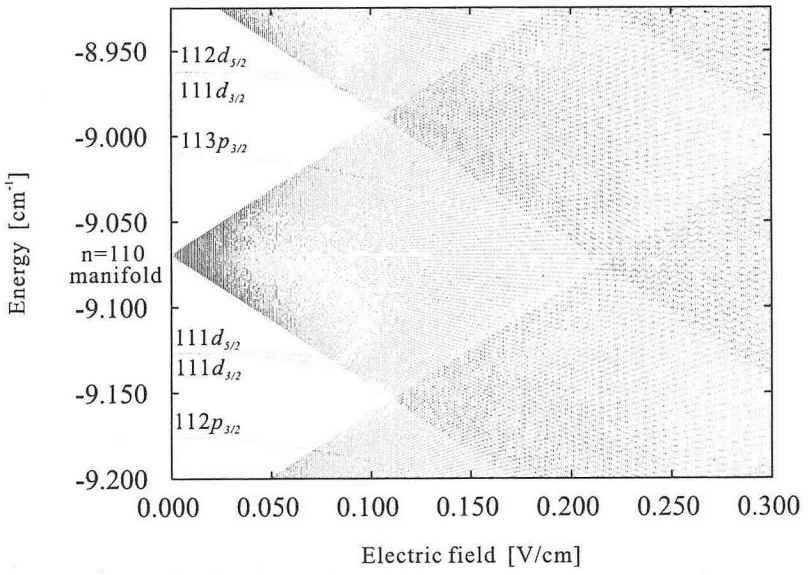

Figure 5: Calculated Stark energy structure of ^{85}Rb for $n = 110, |m_j| = 3/2$.

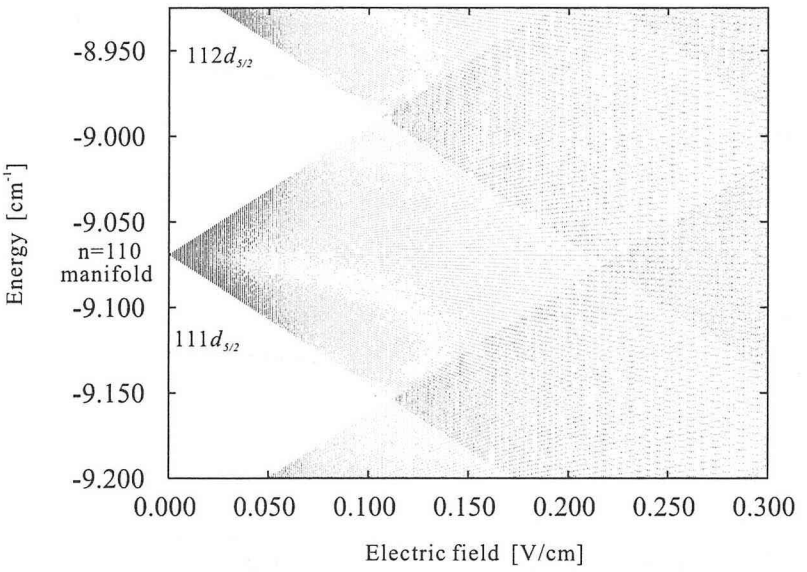

Figure 6: Calculated Stark energy structure of ^{85}Rb for $n = 110, |m_j| = 5/2$.

3.3 Time evolution of highly excited atoms in an electric field

We develop the formalism in which time evolution involving many levels and many avoided crossings can be treated.

We then calculate the adiabatic and non-adiabatic transition probabilities from a p state to the states in the adjacent manifold with this formalism. Since the probabilities of the adiabatic and non-adiabatic transitions depend exponentially on the level separation at the avoided crossing, the comparison of the theoretical calculation with the experimental results is a sensitive test to see the applicabilities of the present theoretical calculations. The tracing of the time evolution in the multi-level formalism is also applied to the level crossing at zero field.

3.3.1 Framework of time evolution involving many levels

To study the adiabatic and non-adiabatic transitions, we first consider the simple case where only two levels cross and the time dependence of their energy levels are arbitrary functions of time t. This simple case has already been studied by Rubmmark *et al.* [16]. We consider a two-level system governed by a Hamiltonian H_0 which depends explicitly on t. We denote the

eigenvalues of H_0 by $\Omega_1(t)$ and $\Omega_2(t)$ and the eigenstates by $|1\rangle$ and $|2\rangle$. The eigenstates are assumed to be independent of t. Next we consider the effect of a perturbation V, which breaks the symmetry of H_0 and has no dependence on t. The Hamiltonian in this case is given in the $\{|1\rangle, |2\rangle\}$ basis

$$H = \begin{pmatrix} \omega_1(t) & \frac{1}{2}|\omega_0|e^{-i\theta} \\ \frac{1}{2}|\omega_0|e^{+i\theta} & \omega_2(t) \end{pmatrix}, \tag{35}$$

where ω_0, $\omega_1(t)$ and $\omega_2(t)$ are written by,

$$\begin{aligned} \frac{1}{2}|\omega_0|e^{-i\theta} &= \langle 1|V|2\rangle, \\ \omega_1(t) &= \Omega_1(t) + \langle 1|V|1\rangle, \\ \omega_2(t) &= \Omega_2(t) + \langle 2|V|2\rangle. \end{aligned} \tag{36}$$

The separation at the center of the avoided crossing is $|\omega_0|$. The time dependent Shrödinger equation,

$$i\frac{d}{dt}|\Psi(t)\rangle = H|\Psi(t)\rangle \tag{37}$$

is then solved by taking,

$$|\Psi(t)\rangle = C_1(t)\exp\left(-i\int_{t_i}^{t} dt'\omega_1(t')\right)|1\rangle + C_2(t)\exp\left(-i\int_{t_i}^{t} dt'\omega_2(t')\right)|2\rangle. \tag{38}$$

Substituting Eq. (38) into Eq. (37) results in

$$i\dot{C}_1(t) = \frac{\omega_0}{2}e^{-i\theta}\exp\left(i\int_{t_i}^{t} dt'(\omega_1(t') - \omega_2(t')\right)C_2(t), \tag{39}$$

$$i\dot{C}_2(t) = \frac{\omega_0}{2}e^{+i\theta}\exp\left(i\int_{t_i}^{t} dt'(\omega_2(t') - \omega_1(t')\right)C_1(t). \tag{40}$$

At the initial time $t = t_i$, the system is assumed to be in the upper eigenstate,

$$|b_i\rangle = \beta_{1i}|1\rangle + \beta_{2i}|2\rangle, \tag{41}$$

where β_{1i} and β_{2i} are determined from the initial condition at $t = t_i$ and $\beta_{1i} = C_1(t_i)$ and $\beta_{2i} = C_2(t_i)$. We are interested in the probability that the final state is in the lower eigenstate $|a_f\rangle$ at $t = t_f$,

$$|a_f\rangle = \alpha_{1f}|1\rangle + \alpha_{2f}|2\rangle. \tag{42}$$

The transition probability is explicitly given by

$$P = |\langle a_f|\Psi(t_f)\rangle|^2 \tag{43}$$

$$= |\alpha_{1f}^* C_1(t_f) + \alpha_{2f}^* C_2(t_f)|^2. \tag{44}$$

Now the formalism is extended to the case with many number of relevant energy states in a time varying electric field, direction of which is arbitrary. Under a pulsed electric field, the Hamiltonian is given by

$$\begin{aligned} H &= \frac{1}{2m}p^2 - 1/r + V_d + \Lambda + F_x(t)x + F_y(t)y + F_z(t)z \\ &= H_0 + F_x(t)x + F_y(t)y + F_z(t)z. \end{aligned} \tag{45}$$

The matrix elements of x and y are calculated as follows.

$$\begin{aligned} & \langle n, \ell, m_\ell | x + iy | n', \ell + 1, m_\ell + 1 \rangle \\ = \; & \langle n, \ell, m_\ell | \hat{x} + i\hat{y} | n', \ell + 1, m_\ell + 1 \rangle \langle n, \ell | r | n', \ell + 1 \rangle \\ = \; & + \sqrt{\frac{(\ell + m_\ell + 2)(\ell + m_\ell + 1)}{(2\ell + 3)(2\ell + 1)}} \langle n, \ell | r | n', \ell + 1 \rangle, \end{aligned} \tag{46}$$

$$\begin{aligned} & \langle n, \ell, m_\ell | x - iy | n', \ell + 1, m_\ell - 1 \rangle \\ = \; & - \sqrt{\frac{(\ell - m_\ell + 2)(\ell - m_\ell + 1)}{(2\ell + 3)(2\ell + 1)}} \langle n, \ell | r | n', \ell + 1 \rangle, \end{aligned} \tag{47}$$

$$\begin{aligned} & \langle n, \ell, m_\ell | x + iy | n', \ell - 1, m_\ell + 1 \rangle \\ = \; & - \sqrt{\frac{(\ell - m_\ell)(\ell - m_\ell - 1)}{(2\ell + 1)(2\ell - 1)}} \langle n, \ell | r | n', \ell - 1 \rangle, \end{aligned} \tag{48}$$

$$\begin{aligned} & \langle n, l, m_\ell | x - iy | n', \ell - 1, m_\ell - 1 \rangle \\ = \; & - \sqrt{\frac{(\ell + m_\ell)(\ell + m_\ell - 1)}{(2\ell + 1)(2\ell - 1)}} \langle n, \ell | r | n', \ell - 1 \rangle. \end{aligned} \tag{49}$$

With these matrix elements, the matrix element $\langle n^* \ell j m_j | F_q q | n^{*\prime} \ell' j' m_j' \rangle$ is expressed as

$$\begin{aligned} & \langle n^* \ell j m_j | F_q q | n^{*\prime} \ell' j' m_j' \rangle \\ = \; & F_q \delta(m_j, m_j') \delta(\ell, \ell' \pm 1) \langle n^* \ell | r | n^{*\prime} \ell' \pm 1 \rangle \\ & \cdot \sum_{m_\ell = m_j \pm m_s} \langle \ell, \frac{1}{2}, m_\ell, m_s | j, m_j \rangle \langle \ell', \frac{1}{2}, m_\ell, m_s | j, m_j \rangle \langle \ell m_\ell | \hat{q} | \ell' m_\ell \rangle, \end{aligned} \tag{50}$$

where $q = x, y, z$ and $\hat{q} = q/|q|$. Thus, all the matrix elements are known in the $|n\ell j m_j\rangle$ basis. We are interested in the transition from an eigenstate in the field F_i to an eigenstate in the field F_f. We write the initial eigenstate as $|n, Z_1, m_j; (F_i)\rangle$ and the final eigenstate as $|\widetilde{n}, \widetilde{Z}_1, \widetilde{m}_j; (F_f)\rangle$. These eigenstates are obtained by the diagonalization of the Hamiltonian matrix at $t = t_i$ and

t_f, respectively,

$$|n, Z_1, m_j; (F_i)\rangle = \sum_{n,j,m_j} u^{n,Z_1,m_j}_{n,\ell,j,m_j}(F_i)|n, \ell, j, m_j\rangle, \tag{51}$$

$$|\widetilde{n}, \widetilde{Z}_1, \widetilde{m}_j; (F_f)\rangle = \sum_{n,j,m_j} u^{\widetilde{n},\widetilde{Z}_1,\widetilde{m}_j}_{n,\ell,j,m_j}(F_f)|n, \ell, j, m_j\rangle. \tag{52}$$

In such a case, it is natural to use the eigenstates $|n, Z_1, m_j; (F_i)\rangle$ as the basis set. The Hamiltonian is diagonalized at $t = t_i$ in the field $F = (0, 0, F_z(t_i))$,

$$\begin{aligned} &\langle n', Z_1', m_j'; (F_i)|H(t_i)|n, Z_1, m_j; (F_i)\rangle \\ &= W_{n,Z_1,m_j}\delta(n, n')\delta(Z_1, Z_1')\delta(m_j, m_j'). \end{aligned} \tag{53}$$

At time t in the field $F(t) = (F_x(t), F_y(t), F_z(t))$, the Hamiltonian matrix elements are given by

$$\begin{aligned} &\langle n', Z_1', m_j'; (F_i)|H(t)|n, Z_1, m_j; (F_i)\rangle \\ &= W_{n,Z_1,m_j}(F_i)\delta(n, n')\delta(Z_1, Z_1')\delta(m_j, m_j') \\ &\quad + \sum_{q=x,y,z} \Delta F_q(t)\langle n', Z_1', m_j'; (F_i)|q|n, Z_1, m_j; (F_i)\rangle, \end{aligned} \tag{54}$$

where $\Delta F_q(t)$ is given by

$$\Delta F_q(t) = F_q(t) - F_q(t_i), \tag{55}$$

and $\langle n', Z_1', m_j'; (F_i)|q|n, Z_1, m_j; (F_i)\rangle$ for $q = x, y, z$ is given by

$$\begin{aligned} \langle n', Z_1', m_j'; (F_i)|q|n, Z_1, m_j; (F_i)\rangle &= \sum_{n,\ell,j,m_j} \sum_{n',\ell',j',m_j'} u^{n',Z_1',m_j'}_{n',\ell',j',m_j'}(F_i)^* u^{n,Z_1,m_j}_{n,\ell,j,m_j}(F_i) \\ &\quad \cdot \langle n', \ell', j', m_j'|q|n, \ell, j, m_j\rangle. \end{aligned} \tag{56}$$

Now that all the matrix elements are obtained, we solve the Shrödinger equation,

$$i\frac{d}{dt}|\Psi(t)\rangle = H(t)|\Psi(t)\rangle, \tag{57}$$

$$|\Psi(t)\rangle = \sum_{n',Z_1',m_j'} C_{n',Z_1',m_j'}(t)\exp(-i\phi_{n',Z_1',m_j'}(t))|n', Z_1', m_j'\rangle, \tag{58}$$

$$\begin{aligned} \phi_{n,Z_1,m_j}(t) &= \int_{t_i}^{t} dt' W_{n,Z_1,m_j}(F_i) \\ &\quad + \sum_{q=x,y,z} \int_{t_i}^{t} dt' \Delta F_q(t')\langle n, Z_1, m_j|q|n, Z_1, m_j\rangle, \end{aligned} \tag{59}$$

$$\begin{aligned} i\dot{C}_{n,Z_1,m_j}(t) &= \sum_{n',Z_1',m_j' \neq n,Z_1,m_j} C_{n',Z_1',m_j'}(t)\exp\{i(\phi_{n,Z_1,m_j}(t) - \phi_{n',Z_1',m_j'}(t))\} \\ &\quad \cdot \sum_{q=x,y,z} \Delta F_q(t)\langle n, Z_1, m_j|q|n', Z_1', m_j'\rangle. \end{aligned} \tag{60}$$

In Eqs. (58) and (60), we sum up only over the states near the avoided crossing of interest, neglecting other states. This results in much smaller dimension of the ordinary differential equations than that with the original basis set and thus saves computing time profoundly. The ordinary differential equations of Eq. (60) are solved by numerical integrations.

The transition probability from an eigenstate $|n, Z_1, m_j; (F_f)\rangle$ at $t = t_i$ to an eigenstate $|\widetilde{n}, \widetilde{Z}_1, \widetilde{m}_j; (F_f)\rangle$ at $t = t_f$ is obtained in the $|n\ell j m_j\rangle$ basis,

$$P_{\widetilde{n},\widetilde{Z}_1,\widetilde{m}_j} = |\langle \widetilde{n}, \widetilde{Z}_1, \widetilde{m}_j | \Psi(t_f)\rangle|^2 \tag{61}$$

$$= \Big| \sum_{n',\ell',j',m'_j} \sum_{n,Z_1,m_j} u^{\widetilde{n},\widetilde{Z}_1,\widetilde{m}_j}_{n',\ell',j',m'_j}(F_f)^* u^{n,Z_1,m_j}_{n',\ell',j',m'_j}(F_i) \cdot C_{n,Z_1,m_j}(t_f) \exp(-i\phi_{n,Z_1,m_j}(t_f)) \Big|^2. \tag{62}$$

The characteristics of our method is as follows: the matrix elements are calculated exactly by the diagonalization method, and thus the energies and couplings between the states are also exact. Since the dimension of the ordinary differential equations are much smaller, the integration is easier, yet accurate enough.

3.3.2 Avoided crossing in the Stark states of ^{85}Rb

Now we apply the theoretical framework developed in the previous section to the avoided crossing of ^{85}Rb between the $113p_{3/2}$ state and the $n = 110$ manifold.

The Stark level structure around the avoided crossing of ^{85}Rb with $|m_j| = 1/2$ is presented in Fig. 7. The $113p_{3/2}$ state and the bluest and also the second bluest states cross each other at $F = 67.2$mV/cm. The calculated adiabatic and non-adiabatic transition probabilities from the $113p_{3/2}$ states at $F = 64.0$mV/cm to the final states at $F = 77.0$mV/cm are presented in Fig. 25 in Sec. 5.4 as a function of slew rate S_s. The non-adiabatic transition begins to occur when the slew rate becomes higher than 100mV/(cmμs). Comparison of the calculated results and the experimental data is discussed later in Sec. 5.4.

3.3.3 Level crossing of manifold near zero field

To investigate the level crossing near zero field, first we consider a hydrogenic atom for simplicity. The Hamiltonian of manifold with the principal quantum number n is expressed in the $|n\ell j m_j\rangle$ basis,

$$\langle n\ell j m_j | H(t) | n\ell' j' m'_j \rangle = W_n \delta(\ell, \ell') \delta(j, j') \delta(m_j, m'_j)$$

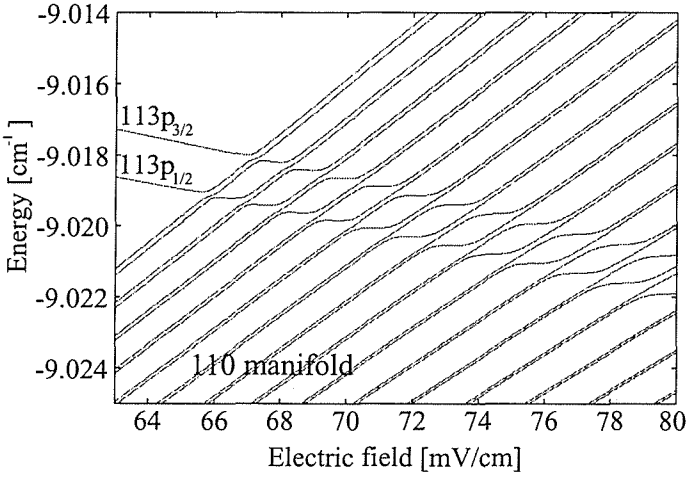

Figure 7: Stark energy structure at the first avoided crossing between the $113p_{3/2}$ and 110 manifold states ($|m_j| = 1/2$).

$$+ \sum_{q=x,y,z} F_q \langle n\ell j m_j | q | n\ell' j' m_j' \rangle. \tag{63}$$

The matrix elements, x, y and z are all commutable, thus there exists a basis $|\boldsymbol{\alpha}\rangle$ such that

$$\langle \boldsymbol{\alpha}|x|\boldsymbol{\beta}\rangle = \xi_{\boldsymbol{\alpha}} \delta(\boldsymbol{\alpha}, \boldsymbol{\beta}), \tag{64}$$
$$\langle \boldsymbol{\alpha}|y|\boldsymbol{\beta}\rangle = \eta_{\boldsymbol{\alpha}} \delta(\boldsymbol{\alpha}, \boldsymbol{\beta}), \tag{65}$$
$$\langle \boldsymbol{\alpha}|z|\boldsymbol{\beta}\rangle = \zeta_{\boldsymbol{\alpha}} \delta(\boldsymbol{\alpha}, \boldsymbol{\beta}). \tag{66}$$

With this basis, the Hamiltonian is also diagonalized,

$$\langle \boldsymbol{\alpha}|H(t)|\boldsymbol{\beta}\rangle = \delta(\boldsymbol{\alpha}, \boldsymbol{\beta}) \left(W_n + F_x(t)\xi_{\boldsymbol{\alpha}} + F_y(t)\eta_{\boldsymbol{\alpha}} + F_z(t)\zeta_{\boldsymbol{\alpha}} \right). \tag{67}$$

All states are orthogonal, and their energies are linear functions of F_q. When the field direction is reversed to the opposite direction, the bluest state therefor becomes the reddest state, the reddest becomes the bluest and so forth. Also the position of manifold is changed from $+(Z_1 - Z_2)$ to $-(Z_1 - Z_2)$ when the field direction is reversed. Figure 8 illustrates the change of an energy level at manifold when the field is reversed from F_i to F_f.

Now we consider the manifold of ^{85}Rb. The quantum defects of s, p and d states of ^{85}Rb are large and these states are separated from the manifold. The states in manifold have only small components of s, p and d state and

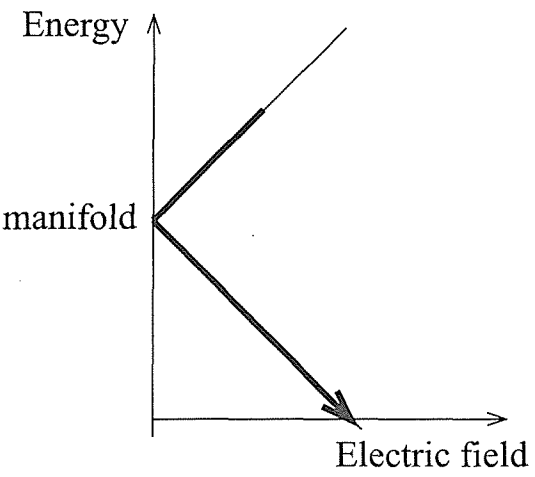

Figure 8: Schematic diagram of the time evolution of a state excited in a negative electric field when the pulsed electric field is driven once to zero field and then to the positive direction.

they mainly consist of higher angular momentum states. For these states, the fine structure interaction is negligible. When the small quantum defect of the f state is ignored, the manifold levels are degenerated at zero field, and the hydrogen approximation is good for the states in manifold.

3.4 Field ionization of highly excited atoms

3.4.1 Ionization by the tunneling process

In this section we calculate the ionization rate by the tunneling process under the hydrogen approximation.

The ionization field values F_c and F_{Z_2} were obtained in Sec. 2 by assuming that the Rydberg atoms are ionized immediately when the electron energy reaches the saddle point of the potential barrier. In reality, atoms are ionized with certain probabilities even in a lower field. Damburg and Kolosov obtained an asymptotic expression of the ionization rate by means of the perturbation theory [23],

$$\Gamma = \frac{(4R)^{2n_2+m+1}e^{-2R/3}}{n^3 n_2!(n_2+m)!} \cdot \left(1 - \frac{n^3F}{4}(34n_2^2 + 34n_2m + 46n_2 + 7m^2 + 23m + \frac{53}{3})\right), \quad (68)$$

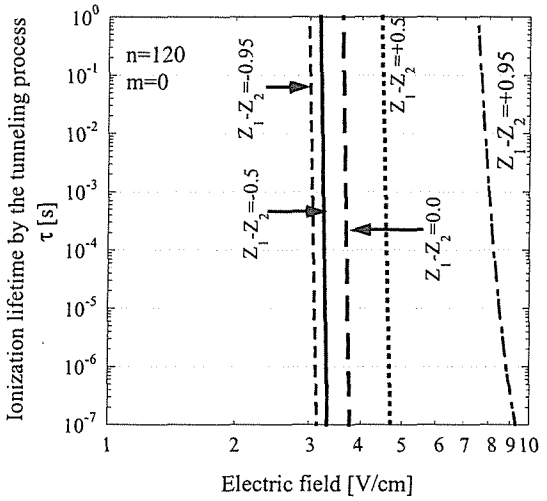

Figure 9: Calculated ionization lifetimes of $n = 120, m = 0$ states for various $Z_1 - Z_2$.

where $R = (-2E_0)^{3/2}F^{-1}$ and E_0 is the energy calculated by the perturbation expansion to the order of F^2. This expression gives very good result at small n_2, *i.e.* a blue state, but it can be used only in a weak filed $F \ll [8n^3(2n_2 + m + 1)]^{-1}$. In order to calculate the ionization rate in a larger field, they analyzed the numerical solutions of the Stark problem for the hydrogenic atom and obtained the semi-empirical expression of Γ,

$$\Gamma = \frac{(4R)^{2n_2+m+1}e^{-2R/3}}{n^3 n_2!(n_2+m)!} \cdot \exp\left(-\frac{n^3F}{4}(34n_2^2 + 34n_2m + 46n_2 + 7m^2 + 23m + \frac{53}{3})\right), \quad (69)$$

where $R = (-2E_0)^{3/2}F^{-1}$ and the energy E_0 is calculated up to the order of F^4 [18]. We note that Γ has n^{-3} dependence. Figure 9 shows the calculated ionization lifetimes of manifold $n = 120$ with Eq. (69). The lifetime decreases quite abruptly with the increase of the field strength, implying that this ionization process has a sharp threshold field F_{th}. Figure 10 shows the thresholds F_{th} of $(n, m) = (120, 0)$, $(120, 1)$, $(108, 0)$ and $(100, 0)$ as functions of the difference of the separation parameters $Z_1 - Z_2$. Here the field F_{th} was defined to the field at which the lifetime τ becomes $10\,\mu$s. The obtained lifetimes do not show any appreciable m dependence. As expected from the classical calculation of F_{Z_2}, blue states have higher thresholds than red ones.

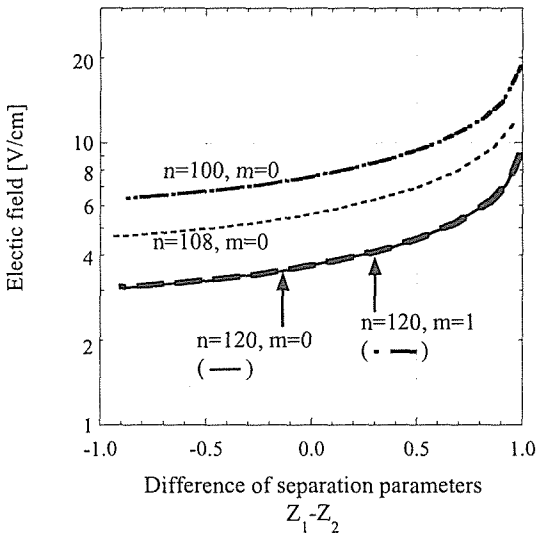

Figure 10: Ionization field value F_{th} expected from the tunneling process.

Values of three ionization fields F_c, F_{Z_2} and F_{th} for the $n = 108$, $m_\ell = 0$ manifold are shown in Fig. 11. The important point here is that F_{th} is higher than F_{Z_2}, and the difference becomes larger for the bluer state.

More exact calculation of the ionization rate with the tunneling process is obtained by using the wavefunction of a state near the core: exact solutions of Shödinger equation in parabolic coordinates can be obtained by a numerical integration method. With these exact solutions, Lec-Koenig and Bachelier calculated the ionization lifetime by the tunneling process [19]. Here we outline their method. For small ξ and η, the wave function in a field F is given by

$$\psi = \sqrt{C(W)^m_{n_1}}(\xi\eta)^{|m|/2}\frac{\exp(im\phi)}{\sqrt{2\pi}}, \tag{70}$$

where $\sqrt{C(W)^m_{n_1}}$ is the normalization factor and called "density of states". For chosen values of F, $|m|$ and n_1, the density of states is a function of the energy W and shows a resonance structure. In the vicinity of a resonance energy W_r, the density of states is expressed by

$$C(W)^m_{n_1} = C(W_r)^m_{n_1}\frac{\Gamma^2/4}{(W - W_r)^2 + \Gamma^2/4}. \tag{71}$$

The lifetime is given by $\tau = 1/\Gamma$.

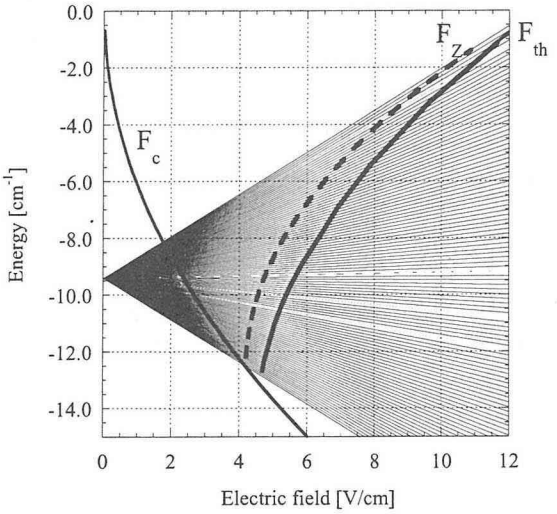

Figure 11: Stark energy shift and the ionization threshold in a hydrogenic atom with $n = 108$, $m_\ell = 0$. The thin lines show the energy levels in an electric field. The three ionization fields F_{Z_2}, F_{th} and F_c (see text for the meaning) are shown by the bold dashed line and the two bold lines, respectively.

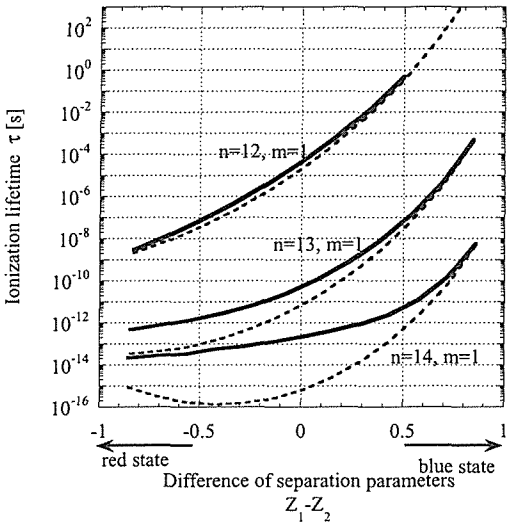

Figure 12: Ionization lifetime by the tunneling process for n=12-14, m=1. The electric field is assumed to be $F = 5 \times 10^{-6}$ [a.u.] = 25.7 kV/cm. The solid lines represent the lifetimes given by the density of states calculation. The dashed lines represent the lifetimes given by the semi-empirical formula Eq. (69).

Following their method, we calculated the lifetimes of Rydberg states at n = 12, 13 and 14($|m|$ = 1), where the electric field was taken to be 5×10^{-6} [a.u.] =25.7 kV/cm. The results are shown in Fig. 12, in which the lifetimes given by Eq. (69) are also presented. The semi-empirical formula Eq. (69) gives shorter lifetime than the exact result from the density of states, especially for the red states. In the case of n=14, $Z_1 - Z_2 \sim 0$, the lifetimes obtained from the two methods differ more than two order of magnitude. For the range of interest here for $\tau \sim 0.1 - 100\,\mu$s, however, the difference is in a factor of $2 \sim 3$. We will discuss the effect of the differnce in Sec. 6.1.

3.4.2 Ionization by the autoionization-like process

In non-hydrogenic atoms, a blue state has probability to interact with red continuum states coming from the higher n manifolds. This interaction causes the ionization of the blue state. This ionization rate of a state $|nZ_1m_j\rangle$

is given by Fermi's Golden Rule,

$$\gamma_d = 2\pi \sum_{Z_1' m_j'} |\langle n Z_1 m_j | V_d | \epsilon Z_1' m_j' \rangle|^2 \quad (72)$$

$$= 2\pi \sum_{Z_1'} | \sum_{j\ell} \langle n Z_1 m_j | n\ell j m_j \rangle \langle n\ell j m_j | V_d | \epsilon \ell j m_j \rangle \langle \epsilon \ell j m_j | \epsilon Z_1' m_j \rangle |^2, \quad (73)$$

where the summation extends over all possible values of Z_1'. Here we have taken advantage of the symmetry of V_d,

$$\langle n\ell j m_j | V_d | \epsilon \ell' j' m_j' \rangle = \delta(j,j')\delta(\ell,\ell')\delta(m_j,m_j')\langle n\ell j m_j | V_d | \epsilon \ell j m_j \rangle. \quad (74)$$

We recall that the diagonal matrix element of the core interaction V_d is given by,

$$\langle n\ell j m_j | V_d | n\ell j m_j \rangle = \frac{-\widetilde{\delta}_{n\ell j}}{n^3}, \quad (75)$$

where $\widetilde{\delta}$ is the magnitude of the difference between the quantum defect δ and its nearest integer. The range of $\widetilde{\delta}$ is $-1/2 < \widetilde{\delta} < +1/2$. This expression is generalized to

$$\langle n\ell j m_j | V_d | n'\ell j m_j \rangle = \frac{-\widetilde{\delta}_{n\ell j}}{(nn')^{3/2}}, \quad (76)$$

since the energy normalization of a discrete wavefunction is given by

$$\int d\tau \varphi_{n'}^* \varphi_n = n^{-3}\delta(n,n'). \quad (77)$$

We note here that the element $\langle n\ell j m_j | V_d | n'\ell j m_j \rangle$ has nonzero value only when $\ell \leq 3$, or for the $s_{1/2}$, $p_{1/2,3/2}$, $d_{3/2,5/2}$ and $f_{5/2,7/2}$ states. Since the energy normalization of a continuum wavefunction is expressed by

$$\int d\tau \varphi_{\epsilon'}^* \varphi_\epsilon = \delta(\epsilon - \epsilon'), \quad (78)$$

the matrix element involving a continuum state is obtained by

$$\langle n\ell j m_j | V_d | \epsilon \ell j m_j \rangle = \frac{-\sin(\widetilde{\delta}_{n\ell j})}{n^{3/2}}. \quad (79)$$

Elements of the unitary transformation $\langle n Z_1 m_j | n\ell j m_j \rangle$ are obtained from the diagonalization procedure. Recall again that V_d is nonzero only at $r \sim 0$, where the shape of the wavefunction does not much depend on the external electric field.

It is noted that the unitary transformation between parabolic and spherical coordinates can be analytically obtained in the hydrogen case. For heavy

alkali atoms such as Rb, however, the fine structure interaction is too large to be neglected, so that m_ℓ is not a good quantum number, and thus we have to use $|n\ell jm_j\rangle$ states as basis states. In the hydrogen case, all states in manifold are degenerated and all the energy eigenstates of the manifold have s, p and d components even in a small field, while, in ^{85}Rb, s, p and d states are not degenerated at manifold, and the eigenstates of the manifold have only small components of low angular-momentum states. Indeed it is shown in the actual numerical calculation that the dominant part of the sum in Eq. (73) comes from $\langle nf_{5/2,7/2}m_j|V_d|\epsilon f_{5/2,7/2}m_j\rangle$. To reflect the real situation more exactly, we use the calculated elements of the transformation from the diagonalization method.

The matrix elements $\langle \epsilon Z_1 m_j|\epsilon\ell jm_j\rangle$ are also obtained by taking into account the difference between the normalization of the unitary transformation for a bound state and that for a continuum one. For a bound state of the hydrogenic atom, the normalization of the unitary transformation is given by

$$\sum_{n_1}\langle n\ell m_\ell|nn_1m_\ell\rangle\langle nn_1m_\ell|n\ell m_\ell\rangle = 1 \quad (n_1 = 0, 1, 2, \cdots, n - |m| - 1), \tag{80}$$

and for a continuum state,

$$\int_{-1}^{+1} d(Z_1 - Z_2)\langle \epsilon\ell m_\ell|\epsilon Z_1 m_\ell\rangle\langle \epsilon Z_1 m_\ell|\epsilon\ell m_\ell\rangle = 1. \tag{81}$$

We replace the summation of Eq. (80) by the integration of $(Z_1 - Z_2)$ and obtain the relation,

$$\langle nn_1m_\ell|n\ell m_\ell\rangle = \sqrt{\frac{2}{n}}\langle \epsilon n_1 m_\ell|\epsilon\ell m_\ell\rangle. \tag{82}$$

This relation is extended further to

$$\langle nZ_1m_j|n\ell jm_j\rangle = \sqrt{\frac{2}{n}}\langle \epsilon Z_1 m_j|\epsilon\ell jm_j\rangle. \tag{83}$$

Substituting the numerically calculated values of $\langle nZ_1m_j|n\ell jm_j\rangle$ into Eq. (73), we obtain γ_d. The maximum value of Z_1' is the value for which $F_{Z_2} = W^2/4Z_2 = W^2/4(1 - Z_1)$, *i.e.* the state just reaches the classical ionization value F_{Z_2}. It is noted here that γ_d has n^{-4} dependence.

In Fig. 13, the calculated lifetimes $\tau_d = \gamma_d^{-1}$ of blue states of ^{85}Rb ($Z_1 - Z_2 = 0.95$) with n=100, 120, 130 and 140 and $|m_j| = 1/2$, 3/2 and 5/2 are presented as functions of field strength. As the electric field increases from zero, the lifetime decreases rapidly. This rapid decrease of the lifetime

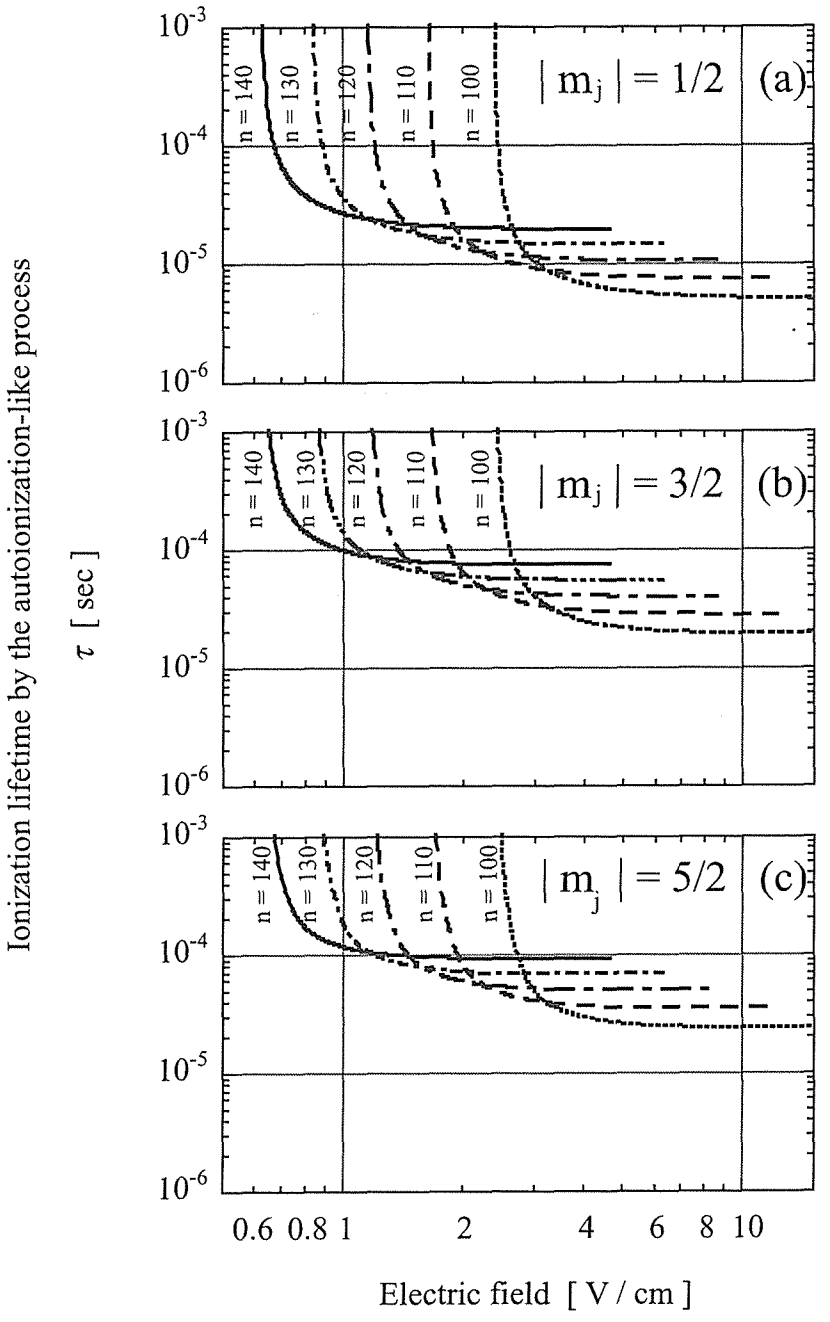

Figure 13: Ionization lifetime of Rydberg states of ^{85}Rb with $Z_1 - Z_2 = 0.95$ by the autoionization-like process.

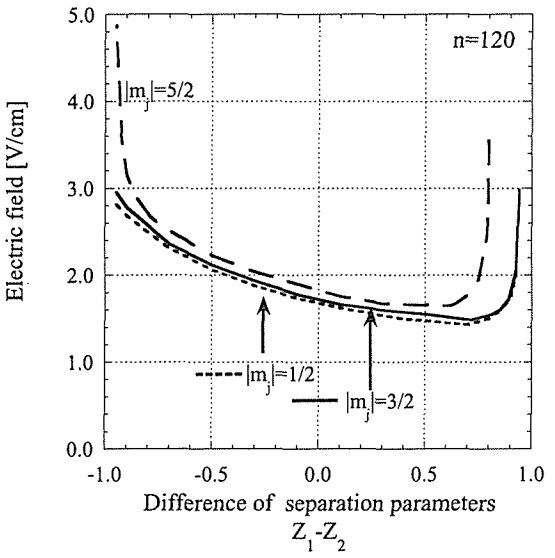

Figure 14: Electric field value F_{10} at which the lifetime of ^{85}Rb with n=120 reaches $\tau = 10\,\mu$sec.

begins at 2.5 V/cm for n=100, at 1.1 V/cm for n=120 and at 0.6 V/cm for n=140. The steep decrease of the lifetime begins at a weaker field for larger n, depending on $|m_j|$. The lifetime reaches a saturated value with increasing the field strength. The saturated lifetime is in the region of 5 - 20 μs, depending on the states. It becomes longer for larger n and $|m_j|$. We denote the field strength as "F_τ" at which the lifetime of the manifold becomes $\tau\,\mu$s. In Fig. 14 plotted are the field values F_{10} as a function of the energy level of the manifold of ^{85}Rb with $n = 120$ for $|m_j| = 1/2$, 3/2 and 5/2. The dependence on $|m_j|$ can be seen only in the extreme blue and red states. The field values F_τ of the states of ^{85}Rb with $|m_j| = 1/2$ are presented as a function of $Z_1 - Z_2$ in Fig. 15 for $n = 120$(top), $n = 108$(center) and $n = 120$(bottom). The ionization field strength by the tunneling process F_{th} is also presented.

The extreme red and blue states have longer lifetimes because they mainly consist of higher angular-momentum components $\ell \geq 4$. Lifetimes of blue states are shorter than those of red ones because blue states have larger components of lower angular-momentum states than red ones. For $n = 120$, the ionization lifetime by the autoionization-like process is longer than 1.0 μs in any field. As n increases, F_{th} and F_{10} become closer. The ionization by the tunneling process becomes dominant in the ionization process with increasing n.

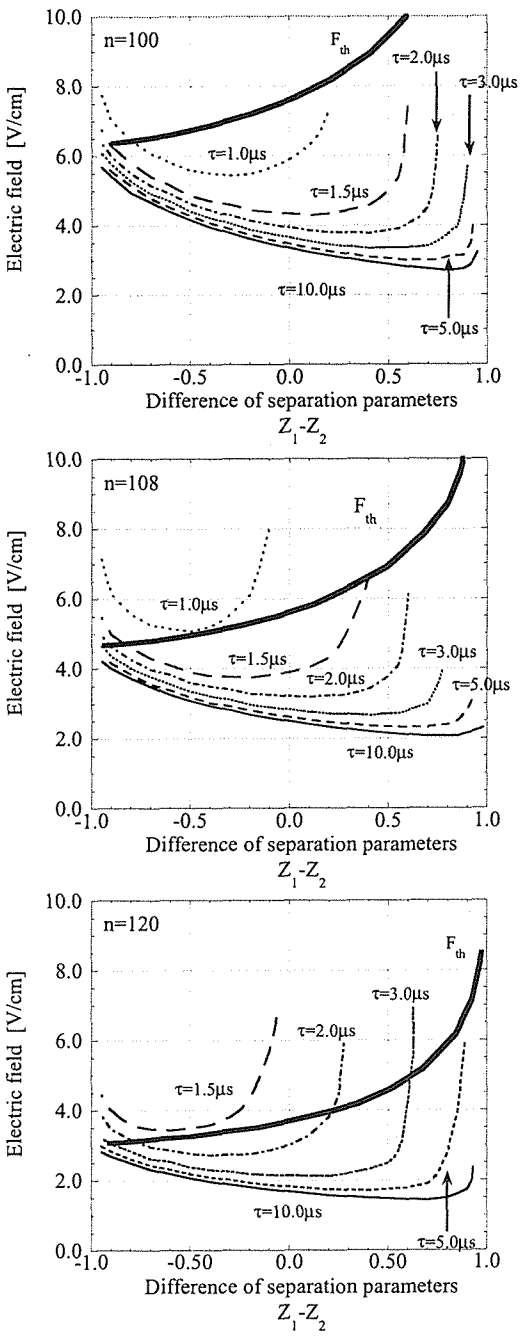

Figure 15: Ionization field values F_τ and F_{th} by the autoionization-like and the tunneling processes, respectively, are shown for the states of ^{85}Rb ($|m_j|$=1/2) with n=100(top), 108(center) and 120(bottom).

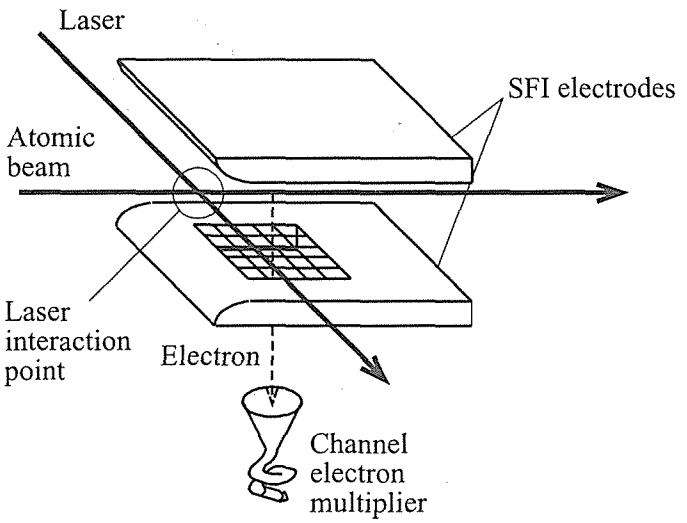

Figure 16: Experimental setup.

4 Apparatus and experimental procedure

4.1 Overview

In this section, apparatus and procedure in the present experiment are described in detail. The overall setup in the present experiment is shown in Fig. 16. Thermal atomic beam of Rb is introduced into the laser interaction area which is included in the field ionization electrodes. The electrons liberated from the field ionization are guided to a channel electron multiplier through two sheets of grid mesh placed on one electrode plate. The whole system is placed in a vacuum chamber. Special care was taken to reduce the stray electric field in the laser interaction and field ionization regions.

4.2 Selective field ionization region

The ionization electrodes consist of two parallel plates of 52 mm length and 40 mm width. Two sheets of fine copper grid mesh are incorporated into the area of $21 \times 22\,\mathrm{mm}^2$ of one of the electrode plates to pass through and detect the electrons. The distance between the electrodes is 24 mm. The diameter of the mesh wire was 0.1 mm so that the transmission through the two mesh becomes 90%.

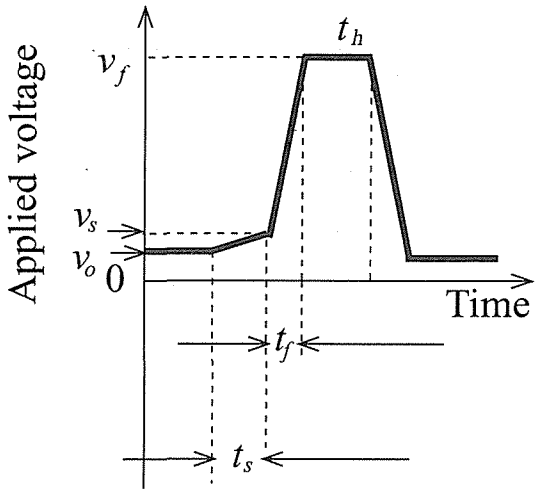

Figure 17: Pulse shape of applied voltage.

4.3 Applied pulse for the field ionization

The pulse voltage applied to the SFI electrodes is shown in Fig. 17. The voltage rises slowly from the offset value v_o to v_s during t_s, and then rises abruptly to v_f during t_f. We call these components "slow" and "fast' component, respectively. The peak field is kept for a time t_h, "holding time", then the voltage goes down to the offset value v_o. The Rydberg atoms are initially excited in a field produced by the applied offset voltage v_o. The voltage v_o is also used to compensate the stray field. The Rydberg atoms are mainly ionized at the fast component during t_f, but a state with a longer lifetime than t_f has some probability to be ionized during the holding time t_h.

The applied electric field strength is given by

$$F_f = v_f/l, \tag{84}$$

where l (24 mm) is the distance between the electrodes. Then the slew rate S_f is given by

$$S_f = F_f/t_f. \tag{85}$$

The pulse sequence is produced with a waveform generator NI5411 (National Instruments) and amplified by fast amplifiers. The output resolution and the maximum update rate of the waveform generator are 12bit (bipolar) and 40 MHz, respectively. The waveform generator has a FIFO memory and a 16 MB memory module, which enable us to store very long arbitrary wave-

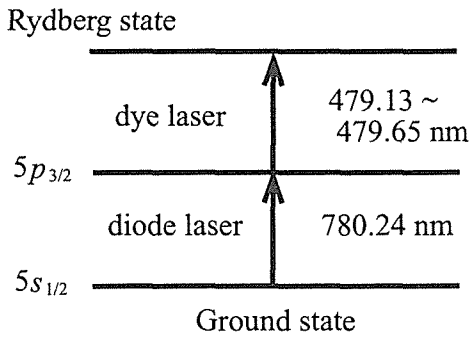

Figure 18: Excitation diagram of ^{85}Rb.

forms on the board and to obtain reliable waveform generation at the maximum update rate. It is possible to vary the slew rates of the fast and slow components independently and to set the offset voltage v_o and the slow component v_s to be positive or negative. The slew rate of the fast component is varied to see the effect of a pulsed field shape on the field ionization characteristics, while that of the slow component is used to drive the excited Stark state to a particular field value adiabatically or non-adiabatically. The slew rate can be increased up to 50 V/(cmμs). The offset voltage is applied to vary the static field at the excitation region of the Rydberg states. Various shape of the field can be applied to the Rydberg atoms.

4.4 Laser setup

Two step excitation was adapted to excite ^{85}Rb atoms from the $5s_{1/2}$ ground state to the Rydberg $n\ell j$ state through second excited state $5p_{3/2}$, as shown in Fig. 18.

A diode laser of Sharp LT025MD0 (780 nm) was used for the first step excitation. The temperature(-17 °C) and the current(135 mA) are controlled to stabilize the wavelength. A dye laser of Coherent 899-21 of coumarin 102 excited by a Kr ion laser was used for the second step excitation. The line widths of the diode laser and of the dye laser are $\sim$ 30 MHz and $\sim$ 500 kHz, respectively. The power of the diode laser was 30 mW at 780 nm, and that of the dye laser was 200 mW at 479 nm with 3 W of the Kr ion laser excitation.

The optical setup is shown in Fig. 19. Two laser beams were mixed by a beam-splitter outside the experimental chamber. The following technique was used to lock the wavelength of the diode laser to the first step excitation wavelength. A small fraction of the laser beam from the beam sampler is

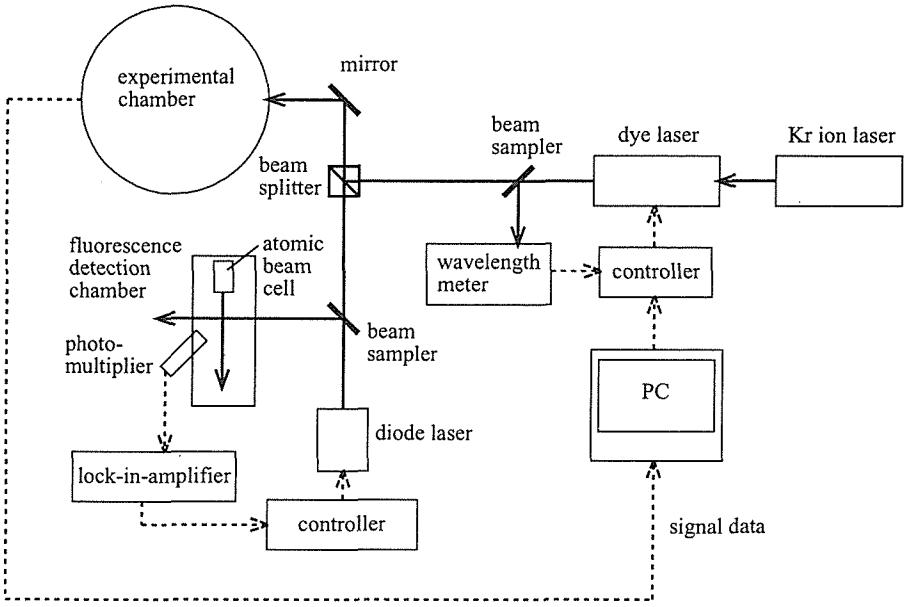

Figure 19: Schematic diagram of the optical setup.

injected perpendicularly (*i.e.* Doppler free) to a thermal atomic beam of Rb in a separate chamber. The ground state atoms were excited to the $5p_{3/2}$ state, and the fluorescence emitted during the deexcitation process to the ground state was detected with a photomutiplier and this signal was used to control the diode current with a lock-in-amplifier so as to keep the fluorescence maximum.

The wavelength of the dye laser was stable enough to be used for our experiment for more than several minutes, without any external control. In order to obtain the longer stability further, the dye laser was controlled with the ionization signal counts of the excited Rydberg states, which is described in more detail in Sec. 4.6.

4.5 Data acquisition

The electron signals from the channel electron multiplier were amplified by a pre-amplifier A250 (Amptek) and a main amplifier AN302/NL (ORTEC) and then fed to a discriminator KN241 (Kaizu). The field ionization signals were then counted through the timing I/O channel in the data acquisition board PCI-6031E (National Instruments), with which the maximum counting rate was 20 MHz. The data were analyzed on-line with the LabVIEW data

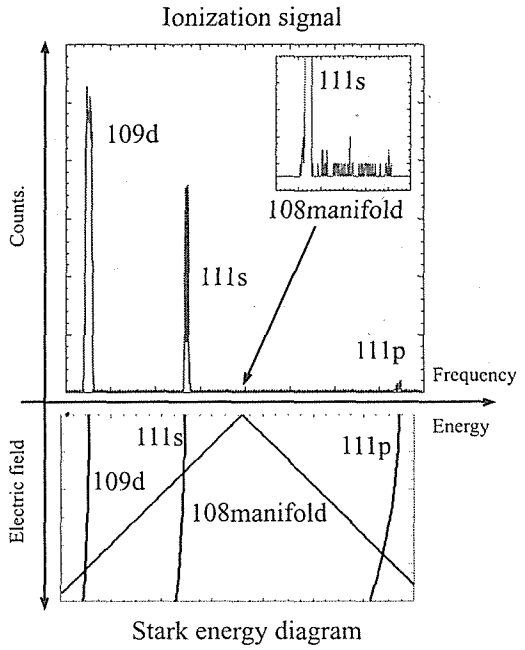

Figure 20: Typical excitation spectrum and corresponding energy levels in the Stark map.

acquisition system on a computer. The whole data were analyzed off-line as well as on-line with LabVIEW programs.

4.6 Experimental procedure

The experiment was carried out with the following procedure.

1)initial setting: The dye laser frequency is set to near the transition of interest, for example, to the $5p_{3/2}$-110 manifold transition with the internal wavelength meter and the controller of the dye laser.

2)laser frequency scanning: The laser frequency is scanned externally by driving the scan-control voltage from a computer. The step size of the scanning is $1 \sim 5$ MHz. During the scanning, the field ionization voltage v_f is kept constant. The ionization signals are counted as the laser frequency is changed. Figure 20 is an example of ionization signal in a wide range of scanning. The Stark energy diagram is also shown with corresponding energy levels.

3)peak holding: When the peak of the signal for the state of interest is

observed, then the scan-control voltage is fixed at the peak position.

4)data taking for ionization spectrum: The field ionization signals are measured by varying the amplitude of the pulse v_f with the same slew rate $S_f = F_f/t_f$, the same offset v_o and the same slow-component v_s. In this process, the ionization counts are measured by changing the ionization field value $F_f = v_f/l$.

5) re-scanning and peak holding: After several ionization spectra are taken, the laser frequency is scanned again. The frequency scanning is carried out in a narrow range around the previous setup frequency. The scan-control voltage is set again to make the signals maximum. This procedure is automatically repeated for some cycles. After that, the parameters, applied field pulse shape, the excited state of interest and so forth, are changed and the procedure is repeated. All these process are controlled by a LabVIEW program system.

5 Experimental results and comparison with theoretical predictions

5.1 Excitation and detection of Rydberg states

Typical excitation spectra of ^{85}Rb are shown in Fig. 21. Without any electric field in the excitation region, the p states and also the manifold states are not excited due to the selection rule for the dipole transitions. Therefore the external field by the offset voltage v_o was applied to the excitation region in order to efficiently excite these states. The strength of the applied field was 70 and 19 mV/cm for the 110 and 116-117 manifold excitations, respectively. The slew rate of the slow component S_s was set to zero. The maximum pulse field was set to 10 V/cm with the slew rate $S_f = 14.4\,\mathrm{V/(cm\mu s)}$ and the holding time t_h was 10 μs.

5.2 Field ionization spectra in a pulsed electric field

Typical ionization spectra are shown in Fig. 22. The left side figures show the spectra for the $113p_{3/2}$ states. The offset electric field by v_o was set to -30 mV/cm. The right side figures show the spectra for the central part of the 120 manifold with $Z_1 - Z_2 \sim 0.2$. The offset electric field by v_o was set to +80 mV/cm. In both cases, the repetition rate of the applied electric field pulse was 3.3 kHz. Here the slew rate of the fast component S_f was $14.4\,\mathrm{V/(cm\mu s)}$, and the holding time t_h was 10 μs. The slew rate of the slow component S_s was set to zero.

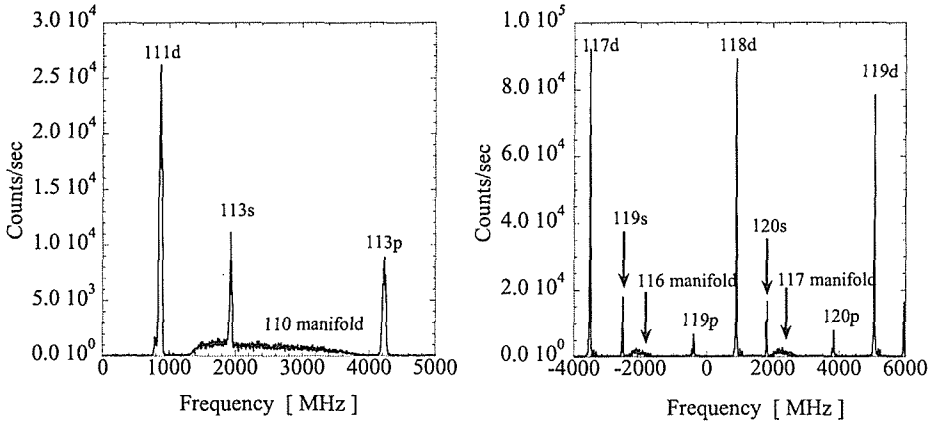

Figure 21: Excitation spectra of ^{85}Rb around $n = 110$ manifold (left) and n =116-117 manifold (right). The atoms were excited in the applied field F=70 mV/cm in the case of $n = 110$ manifold and F=19 mV/cm in the case of n =116-117 manifold in order to excite appreciably many atoms to the states which cannot reach at zero field due to the selection rule of the dipole transition.

The right side of Fig. 22 shows clearly that the field ionization for the manifold states occurs at two separate fields: one is at 1.7 V/cm and the other is 3.7 V/cm. We call the lower peak field "the first field" and the higher one "the second field".

5.3 Characteristics of the pulsed field ionization process

We measured the ionization field values of the states in 120 manifold of ^{85}Rb as a function of the excitation position of the manifold. The field values were measured for the two cases: The Rydberg states were excited at 1) a positive field ($F = +80$ mV/cm) and 2) a negative field ($F = -80$ mV/cm), where the positive field refers to the case at which the ionized electrons correctly drift to the channeltron detector. The atoms excited in the negative field, thus, experienced a pulsed electric field in the reversed direction to the applied static field with the offset voltage. Therefore the atoms were driven first to zero field and then to the ionization region.

The observed ionization field values of states with $n = 120$ are plotted as a function of the excitation position in the manifold $Z_1 - Z_2$ in Fig. 23. In

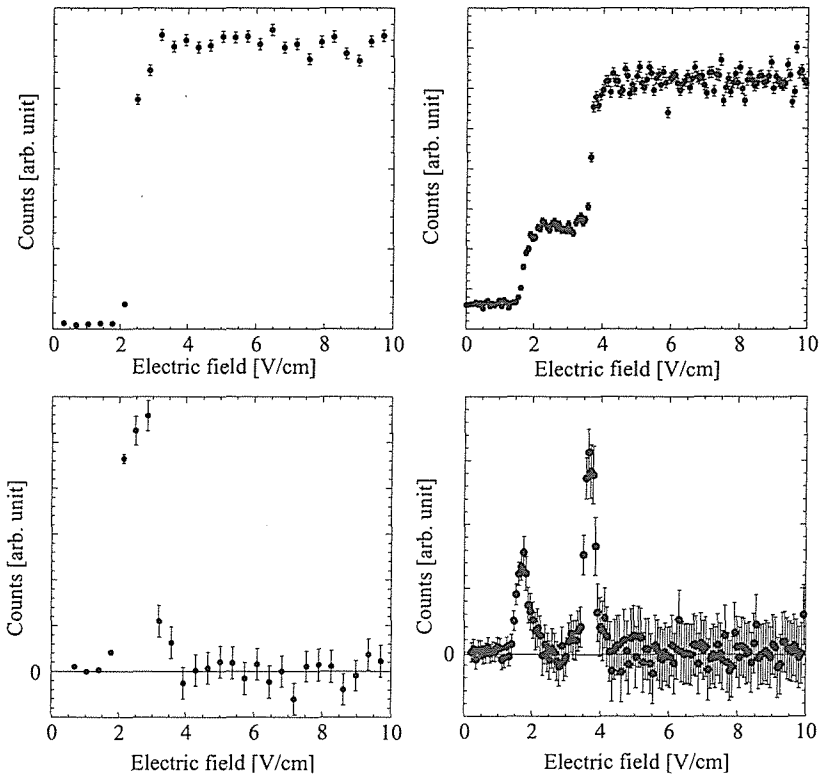

Figure 22: Ionization spectra of the $113p_{3/2}$ state(left) and the 120 manifold states(right). The upper side spectra show the observed raw data, while the lower side spectra were obtained by taking derivatives of the raw data.

Fig. 23 are also presented the calculated ionization field intensities F_{Z_2}, F_{th} and F_{10}.

The upper part of Fig. 23 shows the results of the atoms excited in the positive field direction, while the lower part shows the results of the atoms excited in the negative field direction. In the latter case, the calculated fields were plotted against $-(Z_1-Z_2)$, that is, the value for the position of manifold $+(Z_1 - Z_2)$ were plotted at the corresponding values $-(Z_1 - Z_2)$.

Here the important features are noticed; 1) the first field does not depend on the excited position of the manifold, 2)the second field increases from $\sim$3 V/cm to $\sim$6 V/cm when the excited position is moved more to the bluest side in the positive field case at $F = +80\,\mathrm{mV/cm}$. On the contrary, the second peak field behaves in the opposite direction to the case of positive field when the atoms are excited in the negative field direction at $F = -80\,\mathrm{mV/cm}$.

The calculated field value F_{10} from the autoionization-like process roughly agrees with the observed first-field. The existence of the second field over the first field implies that the lifetime at the first peak field is longer than the pulse rising time $t_f = 0.8\,\mu\mathrm{s}$. This fact is also consistent with the calculated ionization lifetime by the autoionization-like precess.

When atoms with $n = 120$ are excited in the positive field direction at $F = +80\,\mathrm{mV/cm}$, as shown the upper part of Fig. 23, the observed field values for the second peak is in good agreement with theoretical predictions from the tunneling process. The fact that there exists no ionization events above the second field implies that the ionization lifetime at the second field is shorter than the pulse rising time $t_f = 0.8\,\mu\mathrm{s}$. This is also consistent with the calculated results. Form the comparison of these results we can conclude that the second field comes from the ionization by the tunneling process.

Also when atoms are excited to the negative direction at $F = -80\,\mathrm{mV/cm}$, as presented the lower part of Fig. 23, the field values for the second peak are in good agreement with the theoretical predictions if we consider the excited position of the manifold $+(Z_1 - Z_2)$ is reversed to $-(Z_1 - Z_2)$. This observation is consistent with the theoretical predictions that when the atoms are driven to the reversed direction, *i.e.*, once to zero field and then to the increasing opposite field direction for ionization, each state in the manifold is driven to the corresponding state symmetric to the center of the manifold. This is due to the orthogonal properties of the wavefunctions under the hydrogen approximations. Thus the experimental results for both the driving direction are consistent with the theoretical predictions from the tunneling process.

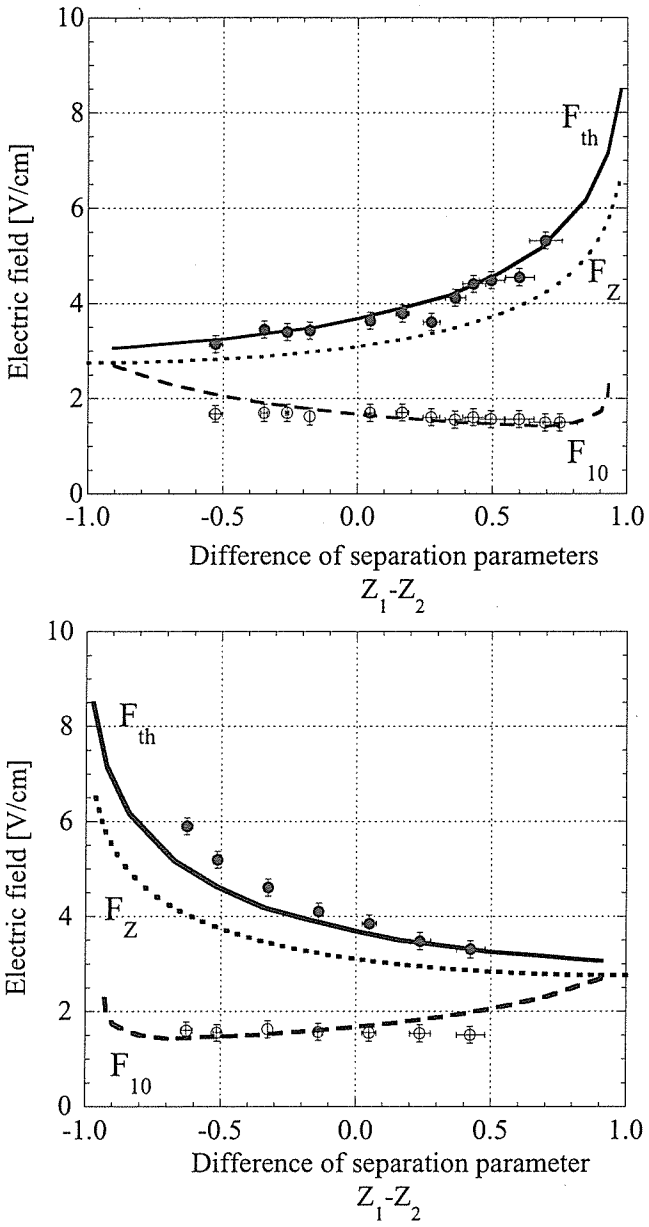

Figure 23: Ionization fields of ^{85}Rb with n=120 are shown as a function of the excited position $Z_1 - Z_2$: the atoms are excited in the positive (the upper) and the negative(the lower) direction (see text in detail). The calculated results are also shown. When the atoms are excited in the negative field direction(the lower), the calculated results are plotted against $-(Z_1 - Z_2)$.

5.4 Adiabatic and non-adiabatic transitions at the first avoided crossing

The experiment on the adiabatic and non-adiabatic transition of the initially excited $113p$ state through the first avoided crossing between the $113p_{3/2}$ state and the bluest state in the 110 manifold was carried out as in the following. The $113p_{3/2}$ state of ^{85}Rb were excited to by two step excitation at the field $F = -30$ mV/cm, where the $113p_{3/2}$ state was well isolated from the manifold. The field was then increased up to $F = -83$ mV/cm, where the $113p_{3/2}$ state merged into the manifold. The applied field was adjusted by the offset voltage v_o and the slow component voltage v_s. Soon after the field reached $F = -83$ mV/cm, pulsed ionization field was applied with a slew rate of the fast component, $S_f = 14.4$ V/(cmμs).

Figure 24 shows two ionization spectra measured in such procedure with the values of the slew rate in slow-component, S_s=0.93 mV/(cmμs) and 80 mV/(cmμs), respectively. It is noted here that the direction of the initial static field is opposite to the direction of the applied ionization field, that is, corresponding to the negative driving as mentioned earlier.

These two ionization spectra show quite different behavior: In the case of the slow slew-rate $S_s = 0.93$ mV/(cmμs), there exist two peaks similar to the case of $n = 120$ manifold. The first-peak field-value coincides with the value expected from the autoionization-like process and the second one to the value expected from the tunneling process. On the other hand, the spectrum in the case of the fast slew-rate $S_s = 80$ mV/(cmμs), there exists only one peak field. These observations are considered to be due to the different transition processes occurred in each case; indeed the second peak corresponds to the adiabatic transition from the isolated $113p_{3/2}$ state to the bluest state in the manifold, while the first peak corresponds to the non-adiabatic transition to the states merged in the manifold as shown in Fig. 7.

The ratios of the counting rates of each peaks to the total sum of both peaks are shown in Fig. 25 as a function of the slew-rate of the slow component. The ratio for the second peak begins to decrease rapidly around S_s=50-100 mV/(cmμs), while that for the first peak increases at around the same slew-rate position. Corresponding results on the transition probabilities from the theoretical calculations are also shown in the same figure. The calculated results are in good agreement with the experimental data, thus showing that the calculated Stark energy structure reproduces well the gap energy between the crossing levels and also that the calculated time evolution along the path of the applied electric field is quite satisfactory for reproducing the transitions at the crossing. It is noted here that the present calculations take into account the multi-level effect and multi-crossing properly near the

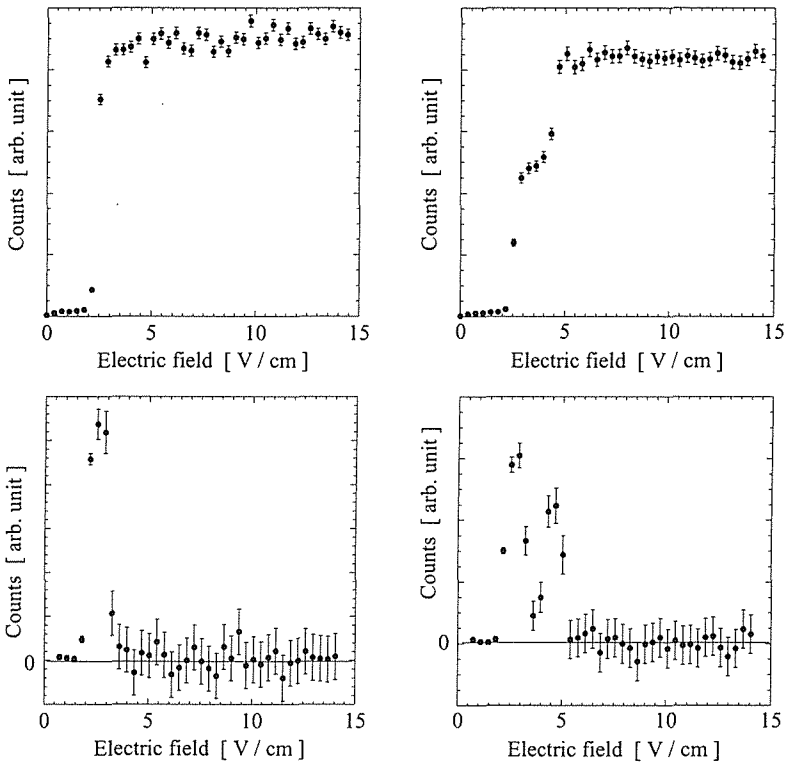

Figure 24: Ionization spectra of the $113p_{3/2}$ states of ^{85}Rb with the slew rate of the slow component $S_s = 80\,\mathrm{mV/(cm\mu s)}$ (left) and $S_s = 0.93\,\mathrm{mV/(cm\mu s)}$ (right). Upper: raw data observed. Lower: derivatives of the raw data. The slow component field was driven from $F = -30\,\mathrm{mV/cm}$ to $F = -83\,\mathrm{mV/cm}$.

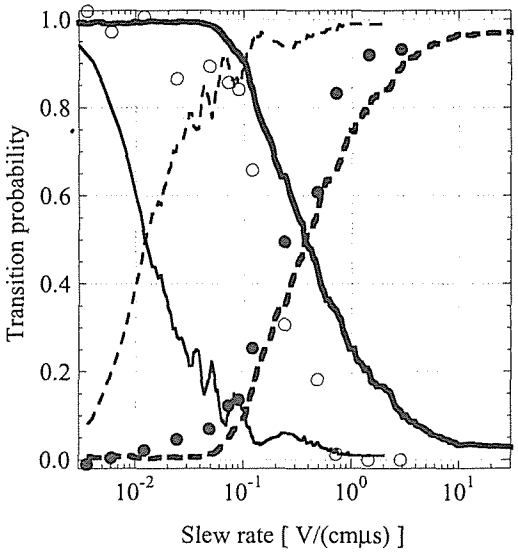

Figure 25: Experimental and theoretical adiabatic and non-adiabatic transition probabilities in the first avoided crossing of ^{85}Rb between the $113p_{3/2}$ and the 110 manifold: The open circles and closed ones show the observed adiabatic and non-adiabatic transition probabilities, respectively. The bold solid line and the bold dashed one show the adiabatic and non-adiabatic transition probabilities calculated with the multi-level time evolution formalism. The thin long-dashed line and the thin solid one show those calculated with the two-level time evolution formalism.

first avoided crossing and that the agreement with the experiment is especially good for this treatment compared to the calculation in which only the first crossing is taken into account.

6 Discussion

6.1 Ionization field of highly excited Rydberg atoms

First we discuss on the ionization process. We measured the electric field strength for ionization of the highly excited Rydberg states in ^{85}Rb and observed two peaks in the ionization field in our investigated field range, up to 18 V/cm. For the 120 manifold, the first field is about 1.7 V/cm, and the second is in the range from 3 V/cm to 6 V/cm. The sharp rise of ionization signal counts at the first field means that the lifetime decreases rapidly around this field and that the lifetime becomes shorter than the pulse holding time $t_h = 10\,\mu$s. The presence of the second field means that the lifetime at the first field is longer than the pulse rising time $t_f = 0.8\,\mu$s. Thus the ionization lifetime at the first field is approximately in the range from $0.8\,\mu$s to $10\ \mu$s. We found no signal-counts increase over the second field value, so that the lifetime at the second field is considered to be shorter than the rising time t_f.

We also measured the ionization field values as a function of the excitation position in the manifold and plotted the data in Fig. 23 together with the calculated results by the tunneling process F_{th} and by the autoionization-like process F_{10}. The second ionization field agrees well with the predictions of the tunneling process. The first peak, on the other hand, is roughly consistent with the prediction of the autoionization-like process. However the observed field values are almost constant with varying position of excitation, which is not in agreement with the predictions of the autoionization process. Also in this peak field there exists appreciable contributions from the blackbody-induced transition to other states from the initially excited state as discussed in the previous work [17]. More detailed discussion on this points will be presented elsewhere.

Underlying field ionization process in this situation can be stated as in the following; as the field increases from zero, atoms begin to be ionized when the field reaches the first ionizing field. The lifetime in this stage is longer than the pulse rising time $t_f = 0.8\,\mu$s, and therefore some of the atoms are not ionized and can survive during t_f. Then with increasing the field, the field reaches the second ionization field F_{th}, where the lifetime by the tunneling process is an extremely rapid function of the applied field so that

all the atoms are ionized at this field.

The theoretical calculations predict that the ionization lifetime by the tunneling process increases in proportion to n^3, whereas that by the autoionization-like process to n^4. Therefore the ionization by the tunneling process becomes more dominant than that by the autoionization-like process for higher n.

Finally we discuss the accuracy of the lifetime calculations by the tunneling process. We have used the semi-empirical formula Eq. (69) to calculate the ionization lifetime of the tunneling process and not used the exact calculation from the density of states Eq. (71). The former predicts shorter lifetime than the latter. The difference of the predicted lifetime seems to be very large especially for the levels approaching the reddest states ("redder states") in a higher field. However this difference does not bring much difference in the ionization field actually as in the following reasoning; as we can see in Fig. 9, the lifetime by Eq. (69) is a very rapid function of the field. At the lifetime around $10\,\mu$s relevant here, the difference of the predicted lifetimes is expected to be within one order of magnitude from Fig. 12. For the state with $n = 120$, $m = 0$ and $Z_1 - Z_2 = -0.5$, the derivative of the lifetime around 1μs is $d\tau/dF = 1 \times 10^{-7}\,\mathrm{s/(mV/cm)}$. Therefore even if the predicted lifetime by Eq. (69) differs by one order of magnitude from the exact value by Eq. (71), the resulting field difference in F_{th} is around $100\,\mathrm{mV/cm}$.

6.2 Time evolution of the multi-level Rydberg system in a pulsed electric filed

We measured the non-adiabatic and adiabatic transition probabilities at the avoided crossings between the $113p_{3/2}$ state and the blue states in the 110 manifold as a function of the slew rate S_s. In this region there exist many Stark levels which avoided-cross each other so that the above first avoided crossing cannot be treated as a single well-separated avoided crossing. This situation is therefore a suitable case for testing the applicabilities of the developed theoretical tracing method for the time evolution of the multi-level Rydberg system in a pulsed electric field.

Moreover the transition probabilities in the avoided crossing depend exponentially on the separation energy between the crossing levels in addition to the crossing field. Therefore this measurement provides a very sensitive test for the underlying calculations of various relevant parameters based on the matrix diagonalization procedure. The calculated adiabatic as well as non-adiabatic transition probabilities are in good agreement with theoretical predictions, thus indicating that our theoretical treatment is quite satisfac-

tory even in such a higher-lying Rydberg system.

Good agreement of the calculated result with the experimental one suggests further that it could be applied to more complicated cases in the time evolution. Suppose, for example, the case that the static electric field applied is a varying function of the position during the excitation and the following ionization process. The position-dependent field component of x or y direction in addition to the z component brings the mixing of m_j in the Stark levels during the flight of the atoms, so that we have to take into account the coherent interactions between the different m_j states. It is then expected that the ionization lifetime by the autoionization-like process may be altered and therefore the field ionization characteristics may also be modified. Since our framework includes phase of wavefunctions properly, we can study the coherent time evolution in such a case without simplification of the system.

The multi-level formalism in the time evolution was also applied to the zero field crossing. Ignoring the fine structure interaction Λ and finite-sized core effect V_d, the states in the manifold are all degenerated as in the case of the hydrogen atom. The states are all orthogonal in any field, and their energies are linear functions of the field. Therefore when the pulsed electric field is reversed from the initial static direction during the ionization process, all the energy states cross at zero field once and then take paths in such a way that the bluest state goes to the reddest state, the second bluest becomes the second reddest, and so forth. The expected trajectory changes with the reversed field direction were actually confirmed by measuring the second ionization field as a function of the excitation position $Z_1 - Z_2$.

6.3 Accuracy and source of error in the diagonalization procedure

We calculated the Stark structure of ^{85}Rb in an electric field by the diagonalization method with the quantum defect theory under the Coulomb approximation. The prediction of ionization lifetime in the autoionization-like process and the tracing of the multi-level time evolution are based on the results by this diagonalization method. We here discuss on the accuracy and the errors in the process of the diagonalization calculation itself.

The diagonal element of the Hamiltonian is evaluated from the quantum defects $\delta_{nj\ell}$. Thus the quantum defects provide the complete specification of the structure and the behavior of a Rydberg state. The uncertainties in them inevitably lead to errors in the Stark structure. Assuming a quantum

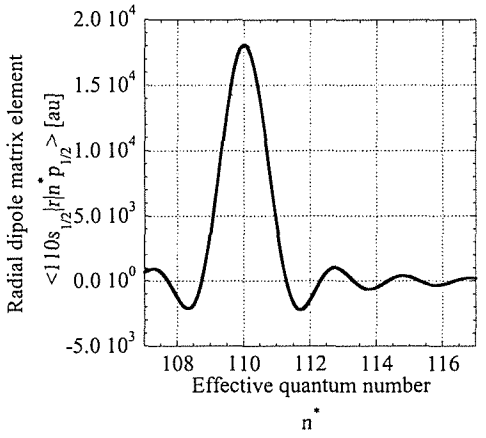

Figure 26: Variation of the radial dipole matrix element $\langle 110s_{1/2}|r|n^*p_{1/2}\rangle$ as a function of the effective quantum number n^*.

defect has a uncertainty $\Delta(\delta)$, the term energy has the error,

$$\frac{\Delta(W)}{W} = \frac{2\Delta(\delta)}{n-\delta}. \tag{86}$$

Errors in the quantum defect values bring possible uncertainties to the results of the Stark structure in two ways: 1) through errors in zero field eigenstates and 2) through errors in the off-diagonal matrix elements. The first error is not serious for large n, because the quantum defects of ^{85}Rb are known within $\Delta(\delta) < 2 \times 10^{-4}$ from Table 1 and thus $\Delta(W) = 1$ MHz at n=110.

Next we consider the second uncertainty, that is, the off-diagonal matrix elements. Figure 26 shows the calculated radial dipole matrix element of ^{85}Rb between the $110s_{1/2}$ state and the n^*p state $\langle 110s_{1/2}|r|n^*p_{1/2}\rangle$. The value of the matrix element varies most rapidly near $n^* = 109.2$, where the matrix element value is 7.6×10^3 [a.u] and the rate of variation is $d\langle|r|\rangle/dn^* = d\langle|r|\rangle/d\Delta(\delta) = 2.0 \times 10^4$. The uncertainty of the quantum defect $\Delta(\delta) = 2\times10^{-4}$, thus, leads to the error of the dipole matrix elements $\Delta(\langle|r|\rangle)/\langle|r|\rangle = 5.3 \times 10^{-4}$.

We also consider the error of calculation of radial matrix elements. In Table 2, we give the calculated radial matrix elements by Eq. (28) and previous results [24]. Our results agree with the previous calculations within 2×10^{-2} for n=40 and 4.5×10^{-4} for $n = 100$. We note here again that the Coulomb approximation is more exact for higher n.

We finally discuss the error due to the truncated basis set. Our treatment becomes less accurate as the electric field increases because the errors

Table 2: Radial matrix elements calculated by this work and other works

Transition $n^*\ell$-$n^{*\prime}\ell'$	$\langle n^*\ell\|r\|n^{*\prime}\ell'\rangle$ this work	$\langle n^*\ell\|r\|n^{*\prime}\ell'\rangle$ (Regemoter *et al.* [24])	$\langle n^*\ell\|r\|n^{*\prime}\ell'\rangle$ (Edmonds and Kelly [25])
39.8p-40p	$+2.2889 \times 10^3$	$+2.288 \times 10^3$	$+2.288 \times 10^3$
39.5p-40p	$+1.7676 \times 10^3$	$+1.767 \times 10^3$	$+1.767 \times 10^3$
38.5p-40p	-2.2163×10^2	-2.214×10^2	-2.215×10^3
99.8p-100p	$+1.4311 \times 10^4$	$+1.431 \times 10^4$	$+8.621 \times 10^4$
99.5p-100p	$+1.1055 \times 10^4$	$+1.105 \times 10^4$	$+1.105 \times 10^4$
98.5p-100p	-1.4211×10^3	-1.421×10^3	$+1.422 \times 10^3$
97.5p-100p	$+5.6658 \times 10^2$	$+5.665 \times 10^2$	$+8.621 \times 10^2$

Table 3: Calculated energy of the bluest and the second bluest states of ^{85}Rb in the 109 manifold

terms in basis set	109-111	108-112	107-113	105-115	103-117
energy [a.u.] (the bluest)	−4.109684	−4.109248	−4.109448	−4.109448	−4.109449
energy [a.u.] (the second bluest)	−4.108837	−4.109119	−4.109288	−4.109288	−4.109290

generally grow with the size of the perturbation. Table 3 shows that energy values of two sample states of ^{85}Rb in $n = 109$ manifold for $|m_j| = 1/2$ converge rapidly with increasing the dimension of the basis set. Since the values converge within 10 kHz over the calculated range of the field up to 0.3 V/cm, the basis set of $105 \leq n \leq 115$ was adapted in the present calculations.

7 Conclusion

We have investigated the properties of highly excited Rydberg states in ^{85}Rb. Specifically the Stark structure and time evolution of highly excited ^{85}Rb Rydberg states in a pulsed electric field have been studied experimentally as well as theoretically. The Rydberg states in ^{85}Rb with the principal quantum number n ranging from 110 to 140 have been excited with the two step laser excitation scheme and field ionization spectra under the pulsed electric field were observed with the ionized electron detection. From the

systematic measurements it was found that in general there exist two peaks in the ionization fields: the lower peak is rather broad and the field value of the peak does not depend on the excitation position in the manifold. The value of the higher peak field, on the other hand, increases with increasing bluer states in the manifold when the pulsed electric field is increased in the same direction with the initially applied static field. However when the pulsed field is increased in the reversed direction to the static field, the peak field decreases with increasing bluer state excitations, showing the opposite behavior to the case in the same field-driving direction.

In order to reveal the origin of these two peak fields in the ionization processes, theoretical calculations of the Stark structure and ionization rates of ^{85}Rb in the electric field have been performed with a computational method based on the Hamiltonian diagonalization. Relevant matrix elements were obtained with the quantum defect theory under the Coulomb approximation.

From these calculations it was found that the excitation position dependence of the higher peaks observed in the field ionization is in good agreement with the predictions from the tunneling process. On the other hand the lower peak behavior is roughly explained from the autoionization-like process together with the effect of the blackbody-induced radiative transitions to the neighboring states from the originally excited states.

In due course of the above investigations, time evolution of the multi-level Rydberg system in a pulsed electric field was also studied to confirm the usefulness and applicabilities of the present method of theoretical calculations. Specifically the transition probabilities in the first avoided crossings of ^{85}Rb between the $113p_{3/2}$ state and the bluest state in 110 manifold was measured and compared with the theoretical predictions obtained from a newly developed formalism on the time evolution of the multi-level Rydberg system. The experimental results are in good agreement with the predictions. The opposite behavior in the excitation-position dependence of the higher ionization peak-field between the driving directions of the pulsed electric field was also found to be well explained with the present theoretical treatment in the time evolution, thus showing the present theoretical treatment is quite satisfactory even in such highly excited Rydberg atoms.

With this method, we can calculate not only the energy levels but also the fundamental physics quantities in an electric filed. By using the quantum defect theory under the Coulomb approximation, all the matrix elements analytically obtained are easy to evaluate and yet accurate enough for the highly excited states with $n > 100$. Further applications of the present theoretical treatment are expected to regions, for example, where the time evolution of a multi-level Rydberg system in a position-dependent static three-dimensional electric field is traced along with an applied pulsed electric field for ionization.

Acknowledgments

The author would like to appreciate kind help and encouragement from Dr. Izumi Ogawa, Dr. Haruhiko Funahashi, Dr. Tomohito Haseyama, Mr. Chikara Ooishi, and Mr. Tomoya Saida.

The author would like to thank Dr. Masaru Tada, Mr. Masahiro Shibata, Mr. Kentaro Kominato, and Mr. Satoru Yamada, for their help in data taking and various discussions.

The author would like to thank Prof. Katsuji Yamamoto for invaluable comments and discussions on theoretical aspects in the present study.

The special thanks should be offered to my academic adviser, Prof. Seishi Matsuki. His guide and suggestion were essential for this work.

References

[1] T. F. Gallagher, *Rydberg Atoms* (Cambridge University Press, Cambridge, England, 1994) and references cited therein

[2] See for example, S. Haroche, *Fundamental Systems in Quantum Optics*, Les Houches 1990 LIII, p.767 (North-Holland, Amsterdam, 1992) and references cited therein

[3] T. W. Ducas *et al.*, *Appl. Phys. Lett.* **35** (1979) 382

[4] H. Figger, G. Leuchs, R. Straubinger and H. Walther, *Opt. Comm.* **33** (1980) 37

[5] P. Goy *et al.*, *Phys. Rev.* A **27** (1983) 2065

[6] S. Matsuki and K. Yamamoto, *Phys. Lett. B* **263** (1991) 523

[7] I. Ogawa, S. Matsuki and K. Yamamoto, *Phys. Rev. D* **53** (1996) R1740

[8] K. Yamamoto and S. Matsuki, *Nucl. Phys. B* **72** (1999) 132

[9] M. Tada *et al.*, *Nucl. Phys. B* **72** (1999) 164

[10] A. Kitagawa, K. Yamamoto and S. Matsuki, *LANL preprint archive* hep-ph/9908445

[11] M. L. Zimmerman, M. G. Littman, M. M. Kash and D. Kleppner, *Phys. Rev. A* **20** (1979) 2251

[12] M. G. Littman, M. M. Kash and D. Kleppner, *Rhys. Rev. Lett.* **41**(1978) 253

[13] D. A. Harmin, *Phys. Rev. A* **26** (1982) 2656

[14] D. A. Harmin, *Phys. Rev. A* **30** (1984) 2413

[15] D. A. Harmin, *Phys. Rev. A* **56** (1997) 232

[16] J. R. Rubbmark, M. M. Kash, M. G. Littman and D. Kleppner, *Phys. Rev. A* **23** (1981) 3107

[17] M. Tada, *Memoirs of the Faculty of Science, Kyoto University, Series of Physics, Astrophysics* (2000) in press

[18] R. J. Damburg and V. V. Kolosov, *J. Phys. B* **12** (1979) 2637

[19] E. Lec-Koenig and A. Bachelier, *J. Phys. B* **13** (1980) 1743

[20] C. J. Lorenzen and K. Niemax, *Phys. Scr.* **27** (1983) 300.

[21] V. A. Davydkin and B. A. Zon, *Opt. Spectrosc.(USSR)* **51** (1981) 13

[22] F. Robicheaux, C. Wesdorp and L. D. Noordam, *Phys. Rev. A* **62** (2000) 43404

[23] R. J. Damburg and V. V. Kolosov, *J. Phys. B* **11** (1978) 1921

[24] H. van Regemertor, Hoang Binh Dy and M. Prud'homme *J. Phys. B* **12** (1979) 1053

[25] P. J. Edmomds and A. R. Tra-Minh N, *J. Phys. B* **11** (1979) L651